OPEN ACCESS

Original research

Identification of bacterial lipopeptides as key players in IBS

Camille Petitfils,[1] Sarah Maurel,[1] Gaelle Payros,[1] Amandine Hueber,[2,3] Bahija Agaiz,[1] Géraldine Gazzo ,[4] Rémi Marrocco,[5] Frédéric Auvray,[1] Geoffrey Langevin,[6] Jean-Paul Motta ,[1] Pauline Floch,[1,7] Marie Tremblay-Franco,[8,9] Jean-Marie Galano,[6] Alexandre Guy,[6] Thierry Durand,[6] Simon Lachambre,[5] Anaëlle Durbec,[2,3] Hind Hussein ,[10] Lisse Decraecker,[10] Justine Bertrand-Michel,[2,3] Abdelhadi Saoudi,[5] Eric Oswald,[1,7] Pierrick Poisbeau,[4] Gilles Dietrich ,[1] Chloe Melchior,[11,12,13] Guy Boeckxstaens ,[10] Matteo Serino ,[1] Pauline Le Faouder,[2,3] Nicolas Cenac [1]

► Additional supplemental material is published online only. To view, please visit the journal online (http://dx.doi.org/10.1136/gutjnl-2022-328084).

For numbered affiliations see end of article.

Correspondence to
Dr Nicolas Cenac, INSERM, Toulouse CS 60039, Occitanie, France; nicolas.cenac@inserm.fr

CP and SM are joint first authors.
PLF and NC are joint senior authors.

Received 16 June 2022
Accepted 27 September 2022
Published Online First 14 October 2022

ABSTRACT

Objectives Clinical studies revealed that early-life adverse events contribute to the development of IBS in adulthood. The aim of our study was to investigate the relationship between prenatal stress (PS), gut microbiota and visceral hypersensitivity with a focus on bacterial lipopeptides containing γ-aminobutyric acid (GABA).

Design We developed a model of PS in mice and evaluated, in adult offspring, visceral hypersensitivity to colorectal distension (CRD), colon inflammation, barrier function and gut microbiota taxonomy. We quantified the production of lipopeptides containing GABA by mass spectrometry in a specific strain of bacteria decreased in PS, in PS mouse colons, and in faeces of patients with IBS and healthy volunteers (HVs). Finally, we assessed their effect on PS-induced visceral hypersensitivity.

Results Prenatally stressed mice of both sexes presented visceral hypersensitivity, no overt colon inflammation or barrier dysfunction but a gut microbiota dysbiosis. The dysbiosis was distinguished by a decreased abundance of *Ligilactobacillus murinus*, in both sexes, inversely correlated with visceral hypersensitivity to CRD in mice. An isolate from this bacterial species produced several lipopeptides containing GABA including C14AsnGABA. Interestingly, intracolonic treatment with C14AsnGABA decreased the visceral sensitivity of PS mice to CRD. The concentration of C16LeuGABA, a lipopeptide which inhibited sensory neurons activation, was decreased in faeces of patients with IBS compared with HVs.

Conclusion PS impacts the gut microbiota composition and metabolic function in adulthood. The reduced capacity of the gut microbiota to produce GABA lipopeptides could be one of the mechanisms linking PS and visceral hypersensitivity in adulthood.

WHAT IS ALREADY KNOWN ON THIS TOPIC

⇒ Intestinal microbiota dysbiosis is associated with IBS symptoms.
⇒ Perinatal stress is a major risk for the development of IBS in adulthood.
⇒ A bacterial lipopeptide, C12AsnGABA, possesses analgesic properties against capsaicin-induced visceral hypersensitivity in mice.

WHAT THIS STUDY ADDS

⇒ In mice, prenatal stress at the end of the gestation induced IBS-like symptoms in adulthood.
⇒ Abundance of *Ligilactobacillus murinus* is inversely correlated to visceral sensitivity to colorectal distension.
⇒ *L. murinus* produce several lipopeptides containing GABA, whose concentration is decreased in prenatally stressed mice.
⇒ GABA-lipopeptide concentration is decreased in faeces of patients with IBS compared with healthy volunteers.

HOW THIS STUDY MIGHT AFFECT RESEARCH, PRACTICE OR POLICY

⇒ Treatment of patients with IBS with lipopeptides containing GABA could be used to decrease visceral pain.
⇒ Quantification of lipopeptides containing GABA could be used to develop personal therapy.
⇒ Lipopeptide-producing bacteria cultured with GABA could represent a novel therapeutic approach in IBS.

Check for updates

To cite: Petitfils C, Maurel S, Payros G, *et al*. *Gut* 2023;**72**:939–950.

INTRODUCTION

IBS affects ∼11% of the world population and is one of the most common causes of gastroenterology consultation.[1] This functional intestinal disorder is characterised by repeated periods of abdominal pain and transit changes (constipation, diarrhoea or an alternate of both). Risk factors for IBS encompass infection, female sex and stress. Indeed, stressful events deeply impact body functions and have been linked to increased IBS symptom severity.[2–4] Recent literature has shown that early-life adverse events have consequences on the onset of chronic non-communicable diseases in adulthood such as IBS.[5–7] In 2012, Bradford *et al* showed that patients with IBS reported more early-life stressors than

healthy subjects, linking early-life adverse events and IBS onset in adulthood.[8] Because events occurring before birth can hardly be included in questionnaires, the effects of in utero events on intestinal dysfunction and IBS symptoms remain unexplored.

In murine models, stress in pregnancy results in gut microbiota dysbiosis in mother and offspring.[9] In patients with IBS, dysbiosis has been reported, but there is a discrepancy in the bacterial composition between studies. For instance, in IBS-D, Tap and colleagues quantified an increase in *Bacteroides*,[10] while Su and collaborators described a decrease in the same IBS subtype.[11] In IBS, a lot of studies investigated the taxonomic composition of the microbiota, but few studies have investigated active genes, proteins or metabolites.[12] However, to better understand the role played by microbiota in host function, studying the molecules produced by the microbiota rather than composition may be more relevant. Indeed, although the taxonomic composition of the human microbiota varies tremendously across individuals, its functional capacity is highly conserved.[13] In a previous study, we highlighted that a probiotic, *Escherichia coli* Nissle 1917, produces a lipopeptide, the C12-asparagine-γ-aminobutyric acid (C12AsnGABA) that decreases both neuronal activation induced by pro-nociceptive molecules in vitro and capsaicin-induced hypersensitivity in vivo.[14] We then determined lipoamino acid (LpAA) and GABA–lipopeptide structures by high-resolution mass spectrometry and developed a quantitative method of newly identified LpAA and lipopeptide–GABA by liquid chromatography coupled to mass spectrometry (LC-MS/MS) in different strains of bacteria.[15 16]

We hypothesised that visceral hypersensitivity in adulthood may originate from functional intestinal microbiota dysbiosis induced by stress in pregnancy. Based on our previous studies demonstrating the ability of lipids to regulate sensory neuron activation,[14 17 18] we assumed that bacteria-derived GABA–lipopeptides may be the link between functional dysbiosis and IBS symptoms. We show that prenatal stress (PS) induces in adult mouse offspring microbiota dysbiosis characterised by a decrease in GABA-containing lipopeptides and visceral hypersensitivity. This decrease is also observed in faeces of patients with IBS.

METHODS

Animal experiments

Six to ten-week-old C57BL/6J mice (Janvier, Saint Quentin Fallavier, France) were used. Mice were raised in sanitary conditions without pathogens, with free access to water and food, and submitted to alternating cycles of 12 hours of light and darkness. After mating (three males and two females per cage), C57BL/6J dams, two mice per cage, were randomly assigned to receive stress from day 13 to day 18 of gestation. The pregnant mice assigned to the stress group experienced bright light (100 W) coupled to restraint in a drilled falcon tube (50 mL; Fischer Scientific, Illkirch, France) for 30 min, 3 times a day, with at least 3 hours between each stress session. Stress efficacy was assessed by controlling faecal output (>4 faecal pellets during the first stress session for the first 2 days). The pregnant mice assigned to the control group were not manipulated. On the last day, gestating mice were put one per cage for natural delivery. The pups were weighed every 3 days to monitor their growth. On postnatal days 21–28, the pups were weaned from their mothers. The offspring between 8 weeks and 11 weeks of age, both male and female, were assessed for visceral sensitivity to CRD, paracellular permeability, colon inflammation, plasma corticosterone concentration, colonic concentration of GABA-containing lipopeptides, and taxonomic, predicted functional analysis and biogeography of the gut microbiota (online supplemental methods). In a second set of experiments, visceral sensitivity to CRD was assessed in PS mice before and 30 min after intracolonic administration of C14AsnGABA (10 µM).

Table 1 Demographic and clinical characteristics of the human cohort

	HV	IBS
N	18	43
Female, n (%)	15 (75)	32 (78)
Age, mean±SD	31.9±12.1	29.6±8.6
Mild IBS, n (%) 75<IBS-SSS<149		7 (16)
IBS–moderate, n (%) 150<IBS-SSS<299		18 (42)
IBS–severe, n (%) IBS-SSS>300		18 (42)

.HV, healthy volunteer; IBS-SSS, IBS Severity Scoring System.

Patients

Patients with IBS and diarrhoea (IBS-D) were recruited according to Rome IV criteria.[19] Clinical examination and standard biological tests were normal. Total colonoscopy and additional tests when necessary had excluded organic disease. Demographic data were prospectively recorded (table 1). IBS symptom severity was assessed by IBS Severity Scoring System (IBS-SSS).[20] This score allows classification of patients with mild (75–174), moderate (175–299) or severe symptoms (>300) (table 1). Healthy volunteers (HVs) were recruited by public advertisement using the gastrointestinal symptom rating scale (GSRS) questionnaire according to European consensus (European cost project).[21] Patients were included at the gastroenterology department of the tertiary care centre (Rouen University Hospital, France) between March 2017 and June 2019 and at the outpatient clinic of the University Hospitals Leuven in Belgium between January 2019 and October 2021.

RESULTS

PS induces visceral hypersensitivity in the adult offspring

We measured the impact of PS on visceral sensitivity in adulthood by measuring visceromotor responses (VMRs) to colorectal distension (CRD). In PS male and female offspring, the VMR and the AUC of the VMR was significantly increased compared with control mice (figure 1A,B). No significant differences in visceral paracellular permeability (online supplemental figure S1A), colon thickness (online supplemental figure S1B) and inflammatory scores at the macroscopic and microscopic level (online supplemental figure S1B) were observed in offspring from stressed dams as compared with controls. PS altered neither basal plasma corticosterone nor the expression of corticosterone receptors in the colon of the adult offspring (online supplemental figure S1C).

At the molecular level, polyunsaturated fatty acid (PUFA) metabolites were quantified in the mouse colons using LC-MS/MS. Mice hierarchical clustering showed that the mice were not separated by their stress status but by their sex (figure 1C), demonstrating that PS had little or no impact on colonic PUFA metabolism. PUFA metabolites hierarchical clustering revealed three different clusters (figure 1C). The first one regrouped products derived from the metabolism of PUFAs by cyclooxygenases (COXs) (PGE_2, TXB_2, 6k-$PGF_{1\alpha}$, $PGF_{2\alpha}$, PGD_2, 8-isoPGA_2, 15-dPGJ_2 and PGE_3), by lipoxygenases (LOXs) (15-HETE, 12-HETE, 9-HODE, 13-HODE, PDx and 14-HDoHE) and by cytochromes epoxygenases (11,12-EET). The means of these metabolites' concentrations were higher in females than in

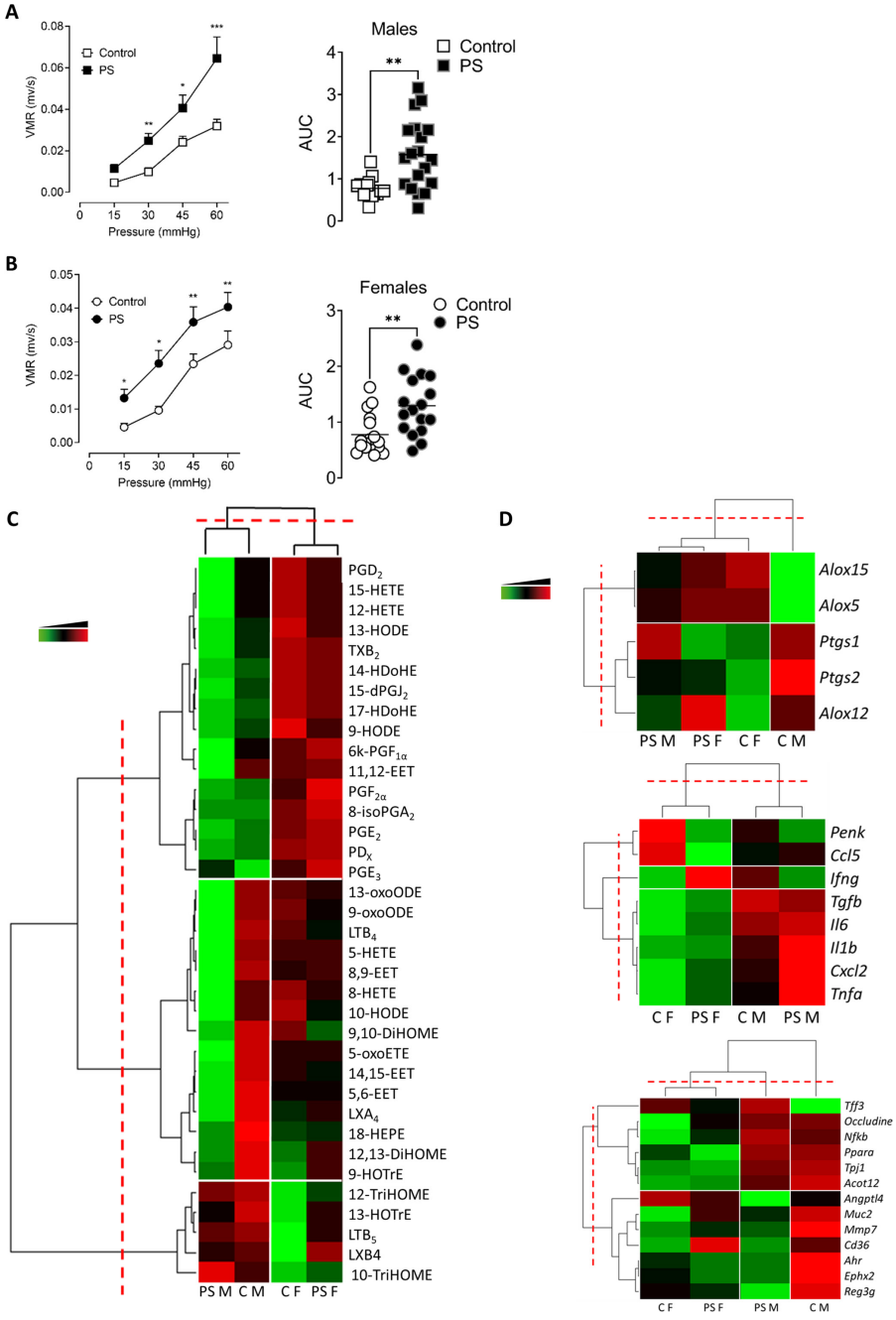

Figure 1 PS induces visceral hypersensitivity in the adult offspring. VMR to colorectal distensions in control (white) or PS (black) mice in response to increasing pressures of distension (15, 30, 45 and 60 mm Hg) was measured in both male (A) and female (B) offspring. Data are expressed as mean±SEM (n=14–19 mice/group, three independent experiments). Statistical analysis was performed using two-way analysis of variance and subsequent Sidak multiple comparison test. *P<0.05, **P<0.01, ***P<0.001 significantly different from the control group. The results are also expressed as AUC presented as scatter dot plot with the mean. Statistical analysis was performed using a Mann-Whitney test. **P<0.01, significantly different from the control group. (C) Heat map of PUFA metabolites quantified by liquid chromatography coupled to mass spectrometry. Data are shown in a matrix format: each row represents a single PUFA metabolite, and each column represents a group of mice: C M=control males, PS M=PS males, C F=control females, PS F=PS females. each colour patch represents the normalised quantity of PUFA metabolites (row) in a group of mice (column), with a continuum of quantity from bright green (lowest) to bright red (highest). The pattern and length of the branches in the dendrogram on the left, reflect the relatedness of the PUFA metabolites, on top the relatedness of the mouse groups. The dashed red line is the dendrogram distance used to cluster PUFA metabolites and mouse groups. (n=15 mice/group, 2 independent experiments). (D) Heatmap of mRNA expression of genes coding for enzymes implicated in PUFA metabolism (top panel), colonic immune response (middle panel) and gut homeostasis (bottom panel). Data are shown in a matrix format: each row represents a single PUFA metabolite, and each column represents a group of mice: CM, CF, PSM and PSF. Each colour patch represents the normalised gene expression (row) in a group of mice (column), with a continuum of quantity from bright green (lowest) to bright red (highest). The pattern and length of the branches in the dendrogram on the left reflect the relatedness of the gene expression on top the relatedness of the mouse groups. The dashed red line is the dendrogram distance used to cluster genes and mouse groups (n=15 mice/group, three independent experiments). AUC, area under the curve; CF, control female; CM, control male; PS, prenatal stress; PSF, prenatal stress male female; PSM, prenatal stress male; PUFA, polyunsaturated fatty acid; VMR, visceromotor response.

males, but no statistical differences were observed between PS and control mice, except for the 11,12-EET, which was significantly decreased in PS male versus control (online supplemental table S1). The second cluster was composed of LOX metabolites (13-oxoODE, 9-oxoODE, 9-HOTrE, LTB4, LXA4, 5-HETE, 5-oxoETE, 8-HETE and 18-HEPA), CYP metabolites (8,9-EET, 9,10-DiHOME, 14,15-EET, 5,6-EET, 12,13-DiHOME) and by the 10-HODE. In this cluster, the concentration of 5-oxoETE, 5-HETE, 8-HETE, LXA4, 10-HODE, 8,9-EET and 14–15-EET was significantly decreased in PS male offspring compared with control mice (online supplemental table S1). Other PUFA metabolites from the LOX pathway (10-TriHOME, 12-TriHOME, LTB5, LXB4 and 13-HOTrE) were portrayed in the last cluster, and their mean concentrations were increased in males compared with females, but no statistical differences were observed (online supplemental table S1). In addition, we quantified mRNA expression of genes coding for the main enzymes implicated in PUFA metabolism. Heatmap of the expression of PUFA metabolising enzymes showed a hierarchical separation of the control males from the three other experimental groups. 5-LOX and 15-LOX expression clustered apart form 12-LOX, COX-1 and COX-2 mRNA expression. Only *Alox5*, which codes for the 5-LOX, was increased in PS males compared with control (online supplemental table S2). PS increases neither proinflammatory lipid mediators nor the enzymes implicated in their synthesis, with the exception of the 5-LOX, in adult male mice.

Then, we assessed the mRNA expression of genes implicated in colonic immune response and homeostasis (figure 1D). Again, hierarchical clustering showed that mice were not separated by their stress status but by their sex and that genes were clustered in three groups *Penk and Ccl5* (cluster 1), *Ifng* (cluster 2), and *Tgfb*, *Il6*, *Il1b*, *Cxcl2* and *Tnfa* (cluster 3). No statistical differences were observed between PS and control adult male and female mice. In agreement, the percentages of $CD8^+$ and $CD4^+$ T cells, regardless of their conventional or memory phenotype, were not significantly different between control and PS mice (online supplemental figure S1D). The expression of genes significant for the epithelium homeostasis grouped the female mice together, unlike males that were separated by the hierarchical clustering, depending on their stress status. Control male mice were represented by an increase in the means of the expression of *Ocln*, *Nfkb*, *Ppara*, *Tjp1*, *Acot12*, *Angptl4*, *Muc2*, *Mmp7*, *Cd36*, *Ahr*, *Ephx2* and *Reg3g*, whereas PS males were represented by an increase of *Tff3*, *Ocln*, *Nfkb*, *Ppara*, *Tjp1* and *Acot12* (figure 1D). In female mice, the means of expression of these genes were lower than in male mice. No statistical difference between control and PS mice was observed (online supplemental table S2).

In conclusion, PS induced visceral hypersensitivity in the absence of any sign of colonic inflammation in adulthood.

PS induces a gut microbiota dysbiosis and alters gut microbiota spatial organisation in adulthood

The 16S RNA analyses of the faeces revealed a shift in the gut microbiota composition in PS mice that differed in male and female offspring. In males, PS mice showed a higher relative abundance of *Clostridium clostridioforme*, *Deltaproteobacteria*, *Desulfovibrionales* and *Blautia*, while the relative abundance of *Desulfovibrio* and Desulfovibrionaceae as well as *Tyzzerella* and *C. colinum* was higher in control mice (figure 2A). In females, the relative abundances of taxa from *Bacteroidetes* and *Verrucomicrobia* phyla were higher than in control mice (figure 2B). In both PS male and female offspring, the relative abundance of *C. clostridioforme* was higher, whereas the relative abundance of *Lactobacillus animalis* was lower (figure 2A,B). These taxonomical differences were in accordance with a significant different and lower overall diversity, mostly based on Chao-1 index, related to rare species, for both PS male and female mice (figure 2C,D). We also performed a phylogenetic investigation of communities by reconstruction of unobserved states (PICRUSt)-based predictive analysis of gut microbial functions. In males, PS mice showed a higher function related to secretion system, whereas control mice displayed higher undefined enzyme families (figure 2E). In females, the predictive gut microbiome did not vary compared with control mice, which showed a higher galactose metabolism (figure 2F).

Beyond taxonomic and functional alteration of the gut microbiota, PS induced a spatial organisational change of the colonic microbiota. In control mice of either sex, bacteria were separated from the epithelial cells by a dense sterile mucus layer (figure 3). In contrast, in PS mice, some bacteria from the gut lumen invaded this layer (figure 3). By quantifying the 16S RNA-labelled pixels inside the mucus layer, we showed that in PS mice, more bacteria crossed the border with the lumen and moved close to the epithelium (figure 3).

Overall, these data show that PS induces gut microbiota dysbiosis and biogeographical changes in adulthood.

Abundance of *L. animalis* is inversely correlated to visceral hypersensitivity

To extract the important differences between prenatally stressed and control mice, we first ran a principal component analysis (PCA) model followed by a partial least-squares discriminant analysis (PLS-DA) model. In both models, the mice were mainly located in within the 95% CIs (black ellipse) (figure 4A,B). The plotted PCA scores showed the aggregation and dispersion of the mice, and no outliers were identified (figure 4). The PLS-DA score plot was fitted on unit variance-scaled data and displays the classification effect. It showed a clear discrimination between the control and PS groups (figure 4B), and the underlying model was validated by a robust ($p<0.05$) permutation test (figure 4C). Seven variables had a variable importance in projection value of ≥ 1 and a p value of ≤ 0.05, showing their importance for group separation in the PLS-DA model. Besides visceral sensitivity (AUC), six bacterial species were identified as important: *Clostridia unclassified*, *L. animalis*, *C. clostridioforme*, *C. colinum*, *Clostridiales unknown* and *Bacteria unclassified* (figure 4D). However, when similar analysis were done on each sex separately, visceral sensitivity was a common variable for separating Ctrl and PS mice, while significant bacteria abundances were different in male and female (online supplemental figure S2). We performed Spearman correlations between these variables to consolidate the link between the identified bacterial species and visceral hypersensitivity. *Clostridia unclassified*, *L. animalis*, *Clostridiales* unknown and *Bacteria* unclassified were inversely correlated to visceral sensitivity (figure 4E). The highest correlation coefficient was reached with *L. animalis* (figure 4E).

In conclusion, visceral hypersensitivity and microbiota composition were the main drivers of the separation between control and PS mice and visceral hypersensitivity strongly correlated to the decreased abundance of *L. animalis*.

Ligilactobacillus murinus concentration is decreased in adult PS faeces

In the mucus of control but not PS mice, we identified by matrix assisted laser desorption ionisation-time of flight (MALDI-TOF) the presence of *L. murinus*, *L. reuteri* and *L. johnsonii/gasseri*. In 2020, the *Lactobacillus* genera regrouped 261 species very diverse from each other on the phenotypical, ecological and genotypical levels.

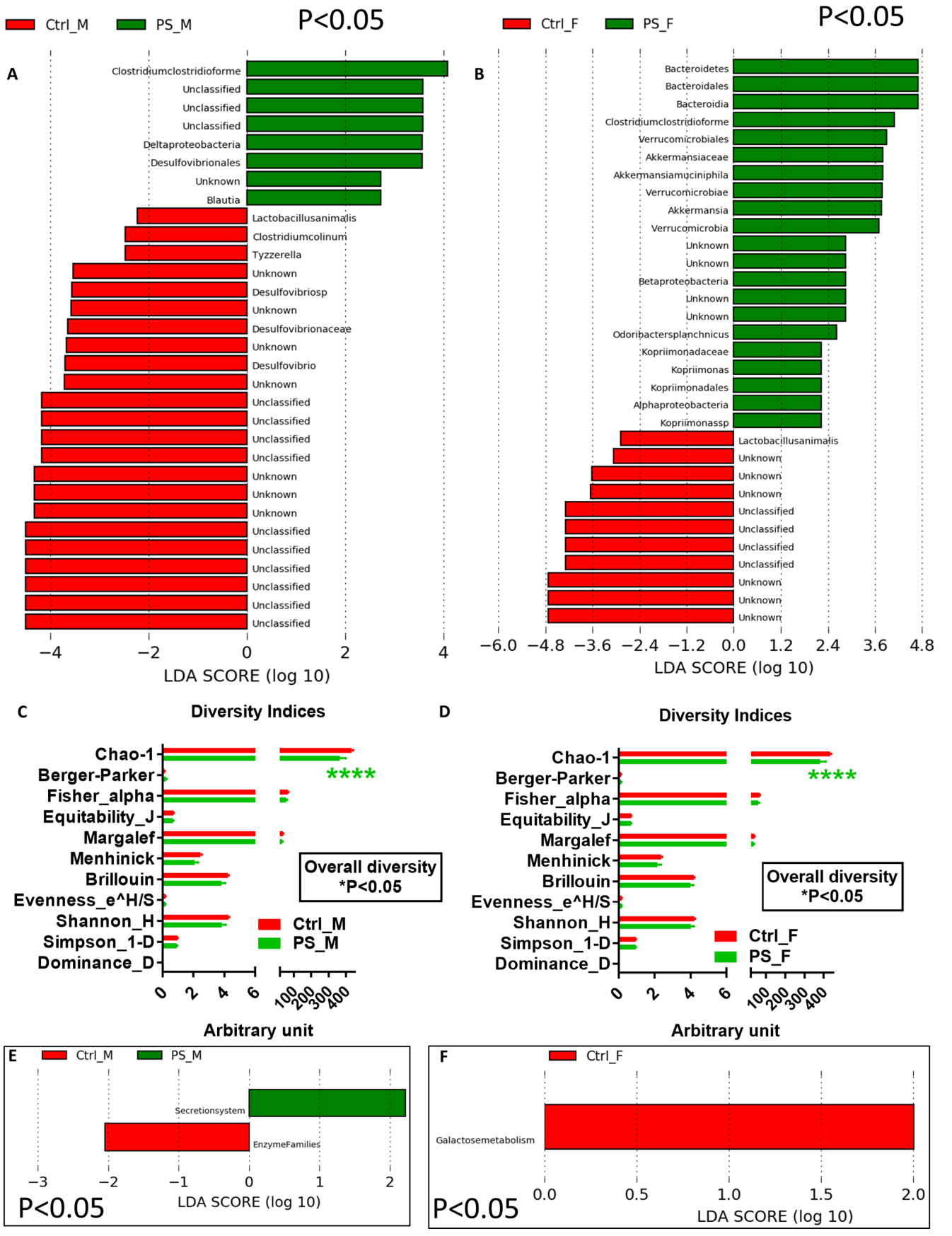

Figure 2 PS induces a gut microbiota dysbiosis both in male and female mice. LDA score in male (A) and female (B) PS mice versus control mice; diversity indices in male (C) and female (D) PS mice versus control mice; PICRUSt-based predicted gut microbial functions in male (E) and female (F) PS mice versus control mice (n=15 mice/group). **** P<0.0001 significantly different from the control group. Ctrl, control; LDA, linear discriminant analysis; PS, prenatal stress; PSF, prenatal stress male female; PSM, prenatal stress male.

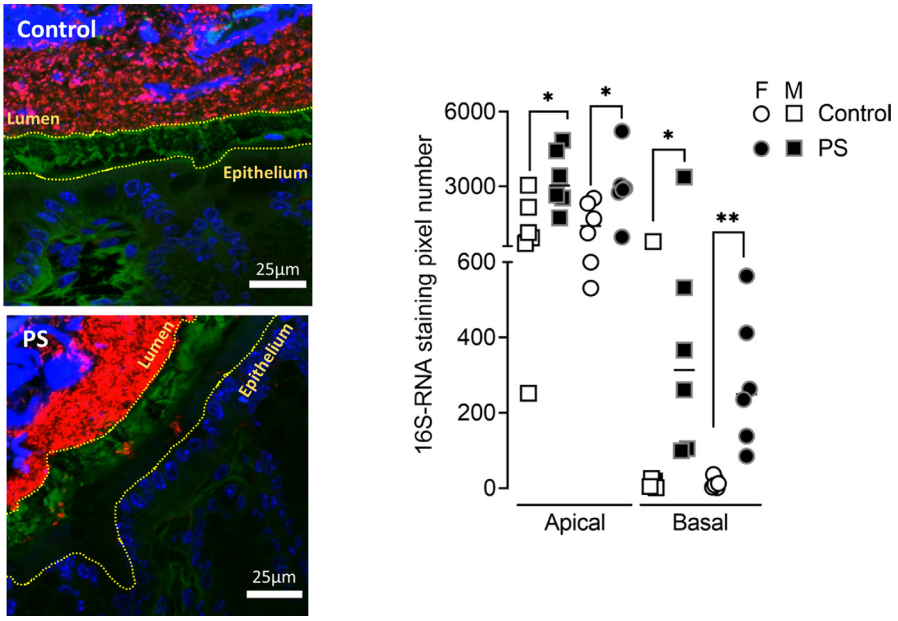

Figure 3 PS alters gut microbiota spatial organisation in adulthood. Bacteria were labelled with the universal probe Eub338 (red); wheat germ agglutinin-Fluorescein-5-isothiocyanate (FITC) was used to stain the polysaccharide-rich mucus layer (green); and the epithelial cell nucleus was stained with 4',6-diamidino-2-phénylindole (DAPI; blue). Bacteria penetration into the mucus was measured in both M (square) and F (circle) control (white symbols) and PS (black symbols) mice by image processing on Fiji by quantifying the number of 16S RNA-labelled pixel between the edge of the lumen and the middle of the mucus (apical) and between the middle of the mucus and the edge of the epithelium (basal). The results are expressed as scatter dot plot with the mean. Statistical analysis was performed using Mann-Whitney test. * P<0.05, **P<0.01, significantly different from the control group. (n=12 mice/group; four images/mice, two independent experiments). F, female; M, male; PS, prenatal stress.

Zheng *et al* re-evaluated the taxonomy of Lactobacillaceae based on whole-genome sequencing and reclassified them into 25 genera.[22] On this basis, *Lactobacillus reuteri* is now classified as *Limosilactobacillus reuteri and L. murinus* as *L. murinus*. The latter is closely related to another species, *L. animalis* and differentiating them from one another remains an issue using the current 16S RNA sequencing pipelines.[23] The same observation is done for probe designing as it is difficult to find species-specific 16S RNA locations. Therefore, it is now recommended to identify them as a single species named *L. murinus/animalis*. As *L. murinus/animalis* was the only identified bacterial species to be correlated with visceral sensitivity, we focused our attention on the role of this bacterium in intestinal homeostasis. Whole-genome sequencing of *L. murinus*, identified in the mice and named strain IRSD_2020, allowed us to determine that it possessed few sequences different from the reference strain DSMZ-20602 (online supplemental figure S3). We then quantified *L. murinus* IRSD_2020 from mice faecal samples by Taqman real-time PCR. *L. murinus* IRSD_2020 quantity was lower in the faeces of PS mice in adulthood and was inversely correlated to the AUC of the visceral sensitivity (online supplemental figure 5A and table S4). The same results were obtained with primers and probe designed for the *L. animalis* strain DSMZ-20602 (figure 5B).

L. murinus produces analgesic lipopeptides

As the abundance of *L. murinus* IRSD_2020 was inversely correlated to the visceral sensitivity, we hypothesised that these bacteria produced a metabolite decreasing visceral sensitivity. Based on our previous study where we described the production of an analgesic GABA-containing lipopeptide by *E. coli* strain[14 14] and on our studies identifying several lipoamines in bacteria,[15 16] we developed a method to quantify the concentration of lipopeptides containing GABA: C12AlaGABA, C12AsnGABA, C14AsnGABA, C14:1AlaGABA, C12ValGABA, C12LeuGABA, C14GABA, C12IleGABA, C14IleGABA, C16LeuGABA, C16PheGABA and C16GluGABA (online supplemental methods). In *L. murinus* IRSD_2020, as no clear production of lipopeptides-GABA was observed (online supplemental figure 6A and table S5) and as these bacteria did not express the enzymes implicated in GABA synthesis, we cultured *L. murinus* IRSD_2020 in the presence of GABA. Under this condition, *L. murinus* IRSD_2020 produced several lipopeptides containing GABA: C16PheGABA, C12AsnGABA, C16GluGABA, C14AsnGABA, C12IleGABA, C14IleGABA and C12AlaGABA (online supplemental figure 6A and table S5). C14:1AlaGABA, C12ValGABA, C12LeuGABA, C14GABA and C16LeuGABA were not quantifiable in *L. murinus* IRSD_2020. The concentrations of C12AsnGABA, C16GluGABA, C14AsnGABA and C14IleGABA were significantly increased in bacteria cultured with 4 mg/mL of GABA (figure 6A). In mouse colons, we quantified C12AsnGABA, C16GluGABA, C14AsnGABA, C12IleGABA and C14IleGABA (online supplemental figure 6B and table S6). C16PheGABA, C12AlaGABA, C14:1AlaGABA, C12ValGABA, C12LeuGABA, C14GABA and C16LeuGABA were not quantifiable in mouse colons. In the colon of PS mice, the concentrations of C12AsnGABA and C14AsnGABA were significantly decreased compared with control (online supplemental figure 6B and table S5). Finally, in the last set of experiments, CRD experiments were performed before and 30 min after intracolonic administration of 10 µM, as already described for the C12AsnGABA,[14] of C14AsnGABA in male and female adult PS mice. Treatment by the lipopeptide decreased the visceral hypersensitivity induced by PS (online supplemental figure 6C and table S5). We identified that *L. murinus* IRSD_2020 produced lipopeptides containing GABA in the presence of GABA. The treatment of sensitive mouse by C14AsnGABA, whose concentration was decreased in their colon, restored a normal visceral sensitivity.

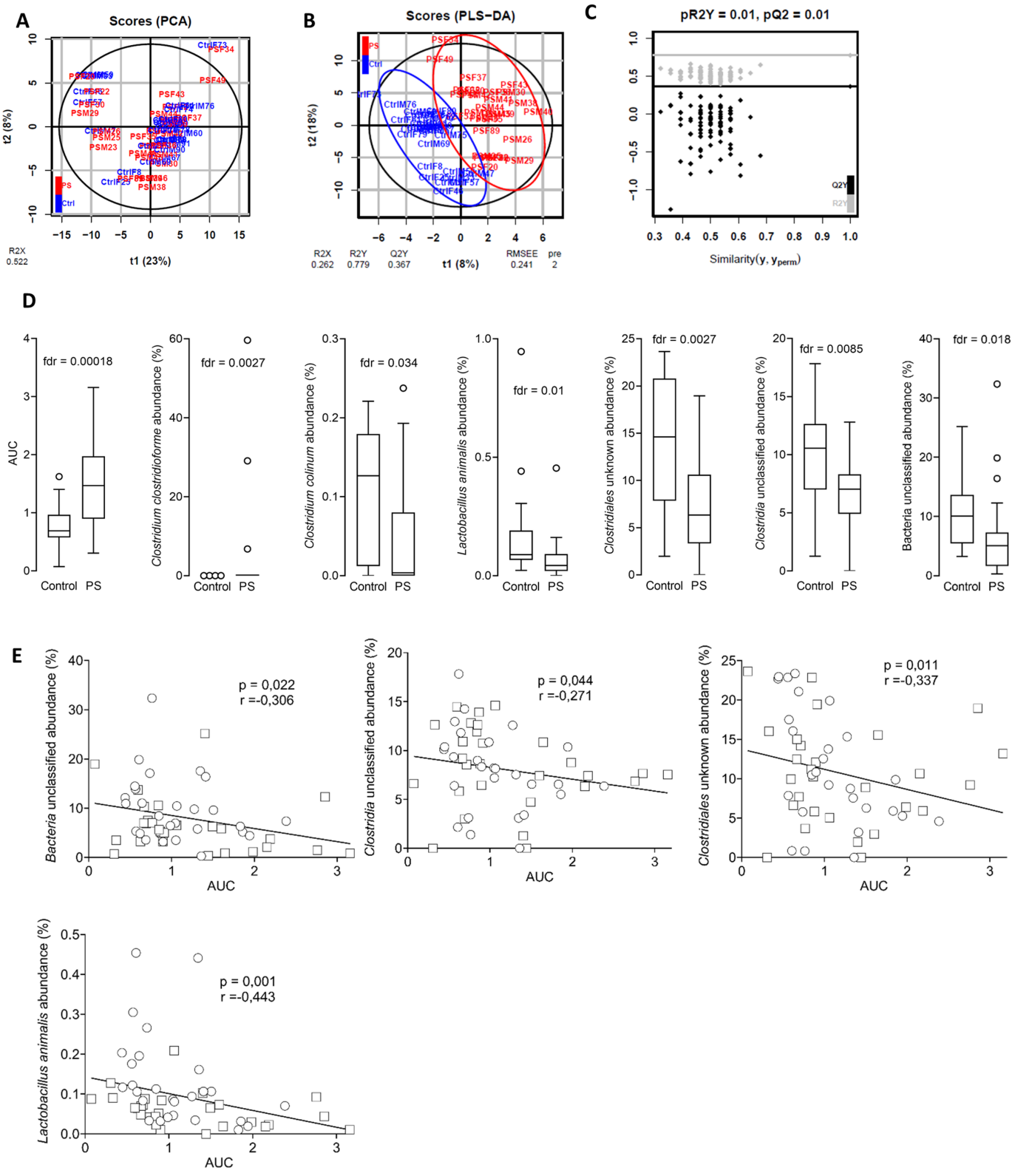

Figure 4 The abundance of *Lactobacillus animalis* is inversely correlated to visceral hypersensitivity in adulthood. Multivariate analysis of the complete cohort: (A) two-dimensional PCA (R2=52%) score plot of data generated from 56 samples (control, n=28, blue; PS, n=28, red). each dot corresponds to an individual. (B) two-dimensional PLS-DA (R2X=26.2%, R2Y=77.9%, Q2=0.367) score plot of data generated from 53 samples (control, n=26, blue; PS, n=27, red). Each dot corresponds to an individual. The black ellipse corresponds to a 95% CI based on the Hotelling's T^2. RMSEE, root mean square error (C) Permutation test result for PLS-DA model validation. (D) Box plots of discriminant (variable importance in projection >1) and significant (false discovery rate (FDR)-corrected p value of Wilcoxon test <0.05) variables. (E) Spearman correlations were used to analyse the correlation between the faecal microbiota abundances and visceral motor response to colorectal distension expressed in AUC, in male (square) and female (circle) offspring. P and R values are indicated on each graph. AUC, area under the curve; PS, prenatal stress.

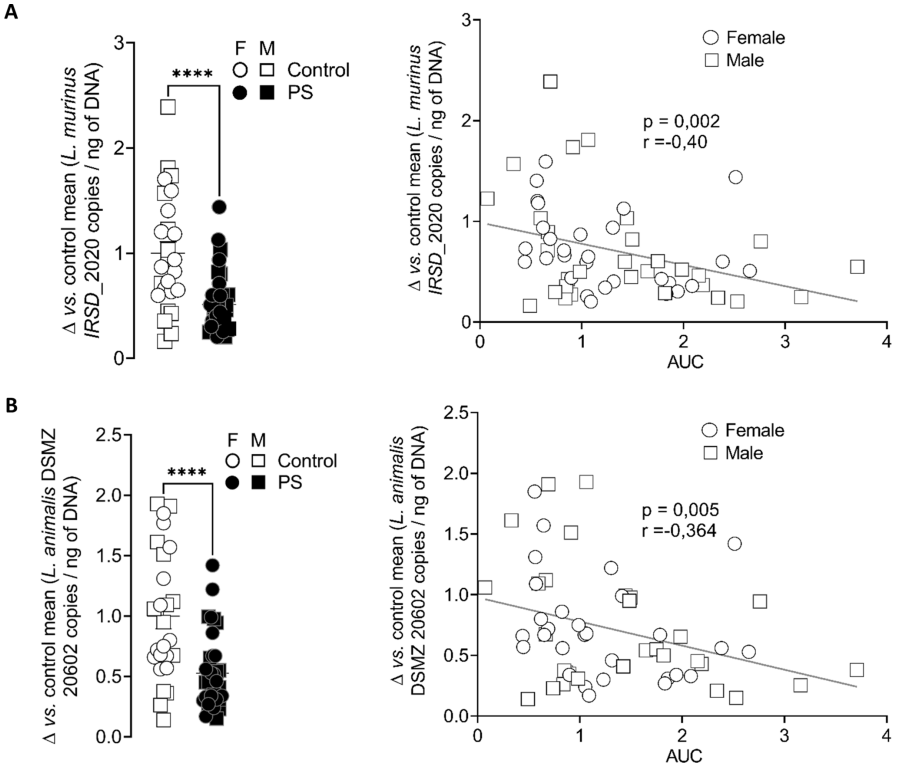

Figure 5 *Ligilactobacillus murinus* IRSD_2020 concentration is decreased in PS mouse faeces. The levels of the *L. murinus* strain IRSD_2020 (A) and of the reference *L. murinus/animalis* strain DSMZ 20602 (B) were quantified by TaqMan real-time PCR in the faeces of control mice (white) or PS mice (black), in the M (square) and F(circle) offspring. Data are expressed as scatter dot plot with the mean. Statistical analysis was performed using Mann-Whitney test. ****P<0.0001, significantly different from the control group (n=27–36 mice/group, three independent experiments). Spearman correlations were used to analyse the correlation between the faecal bacteria quantity and visceral motor response to colorectal distension expressed in AUC, in M (square) and F (circle) offspring. P and R values are indicated on each graph. AUC, area under the curve; F, female; M, male; PS, prenatal stress

Concentration of neuronal activation inhibitory lipopeptides is decreased in faeces of patients with IBS

GABA–lipopeptides were quantified in faeces from patients with IBS and HVs using LC-MS/MS. In contrast to *L. murinus* supplemented with GABA and mouse colon, only the C12AsnGABA and the C16LeuGABA were quantifiable in human faeces. C12AsnGABA was quantifiable in 8 out of 18 HVs and was significantly decreased in patients with IBS (figure 7A). C16LeuGABA was quantifiable in 17 out of 18 HVs and was significantly decreased in patients with IBS (figure 7A). The concentration of C16LeuGABA was significantly inversely correlated to the IBS-SSS and to the abdominal pain score (figure 7B), and did not correlate with SF-36 (online supplemental filgure S8). As C16LeuGABA has never been quantified before, its role on sensory nerves activation is unknown. We next determined whether C16LeuGABA decreases neuronal activation, as previously described for C12AsnGABA.[14] Primary cultures of mouse dorsal root ganglion neurons, activated either by an agonist of the receptor calcium channel TRPV1 (capsaicin) or by a mix of agonists (histamine, serotonin and bradykinin) for G protein-coupled receptors (GPCRs), were treated with C16LeuGABA. Neuron exposure to either capsaicin (500 nM) or the GPCR agonists mix (histamine, bradykinin and serotonin, 10 µM each) induced an increase in calcium flux as shown by the higher % of responding neurons (figure 7C,D). The calcium flux increase induced by both nociceptive stimuli was prevented by C16LeuGABA pretreatment in a dose-dependent manner (figure 7).

DISCUSSION

The onset of IBS in adulthood is associated with a higher number of early-life adverse events.[8] However, due to the lack of data on prenatal period in humans, it is difficult to establish the causal link between stressful events during pregnancy and intestinal homeostasis disruption in adulthood. Here, in a mouse model of PS, we show that the male and female offspring of stressed mothers present the main characteristics of IBS in adulthood: visceral hypersensitivity, no overt colonic inflammation and a gut microbiota dysbiosis. Our results confirmed previous observations made in a rat model of PS where an increase in visceral sensitivity and no change of paracellular permeability have been described.[24 25] In contrast to stress performed in adulthood,[26] we did not observe an increase in plasma corticosterone concentration in PS mice as previously observed in PS rodents.[24 25 27 28] So, corticosterone is probably not implicated in the increase in visceral sensitivity observed in this model at adulthood. Nevertheless, we cannot exclude a long-lasting impact of corticosterone during foetal development and infancy. The gut microbiota of PS mice was, however, significantly altered in both male and female offspring, characterised by an increased abundance of *C. clostridioforme* and a decreased abundance of *L. murinus/animalis*. *C. clostridioforme*, reclassified as *Enterocloster clostridioformis* in 2019,[29] is hardly dissociable from two other bacteria: *C. bolteae* and *C. hathewayi*, all found in human faeces.[30] These three species are therefore usually considered as the *C. clostridioforme* group. A higher abundance of this group in the faeces has been linked to the onset of autism spectrum disorders (ASDs)

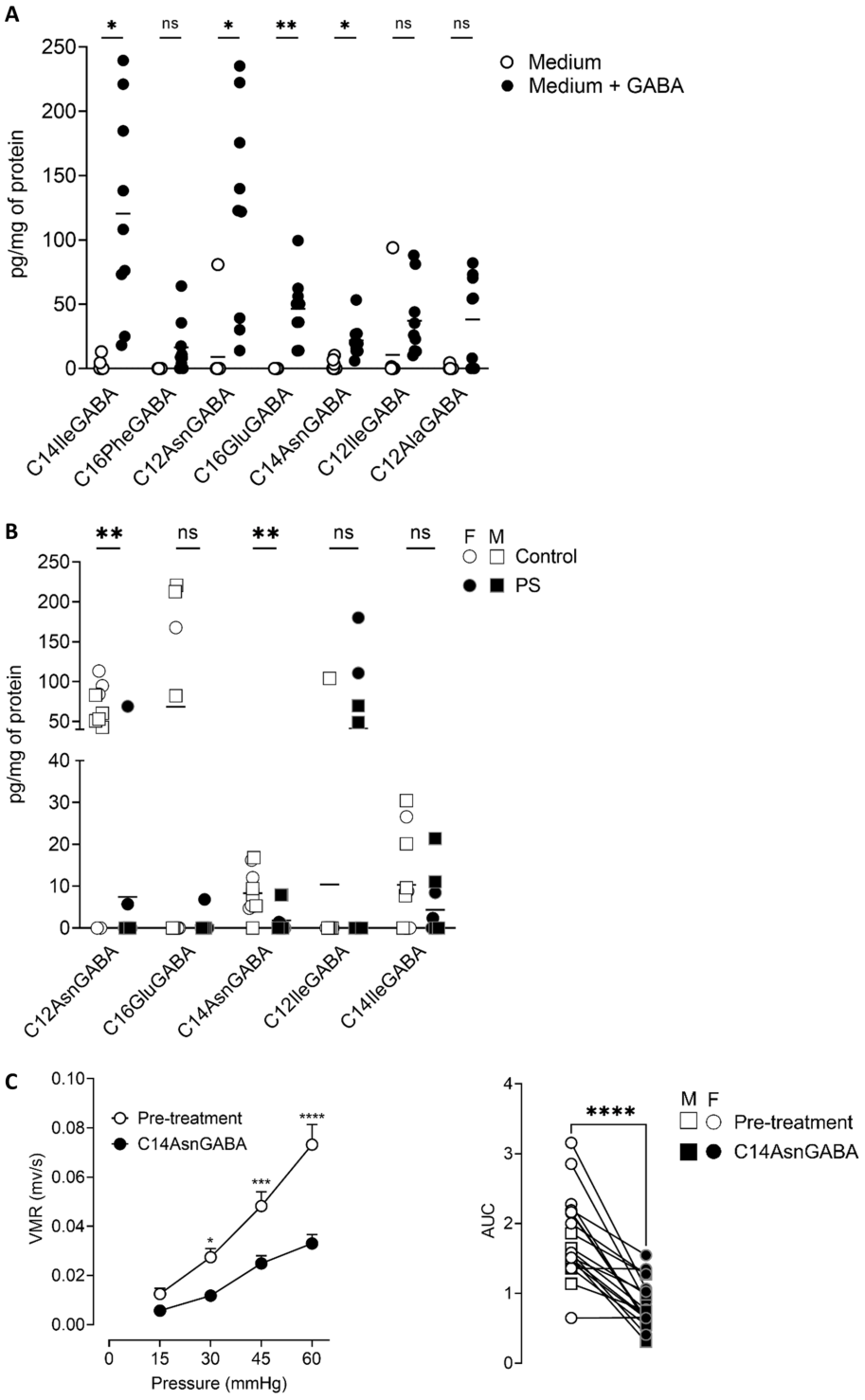

Figure 6 *Ligilactobacillus murinus* IRSD_2020 produces an analgesic lipopeptide. (A) Concentration of lipopeptides quantified by LC-MS/MS in the bacterial pellets of *L. murinus* IRSD_2020 cultivated without (white circle) or with (4 mg/mL) (black circle) GABA . Data are expressed as scatter dot plot with the mean (n=9). Statistical analysis was performed using Mann-Whitney test. *P<0.05, **P<0.01, significantly different from the corresponding *L. murinus* IRSD_2020 without GABA. (B) Concentration of lipopeptides quantified by LC-MS/MS in the colon of M (square) and F (circle) control (white) and PS mice (black). Data are expressed as scatter dot plot with the mean (n=9–10). Statistical analysis was performed using Mann-Whitney test. **P<0.01, significantly different from the corresponding control group. (C) VMR to colorectal distensions in response to increasing pressures of distension (15, 30, 45 and 60 mm Hg) was measured in both M and FM PS offspring. Measurements were done before (white) and after intracolonic administrations of C14AsnGABA (black). Data are expressed as mean±SEM (n=19 mice/group, two independent experiments). Statistical analysis was performed using two-way analysis of variance and subsequent Sidak multiple comparison test. *P<0.05, ***P<0.001, ****P<0.0001 significantly different from the pretreatment group. The results are also expressed as area under the curve (AUC) presented as scatter dot plot with the mean for M (square) and F (circle) mice. statistical analysis was perform using a Wilcoxon test. ****p<0.0001, significantly different from the pretreatment group. F, female; GABA, LC-MS/MS, iquid chromatography–tandem mass spectrometry; M, male; ns, not significant; PS, prenatal stress; VMR, visceromotor response.

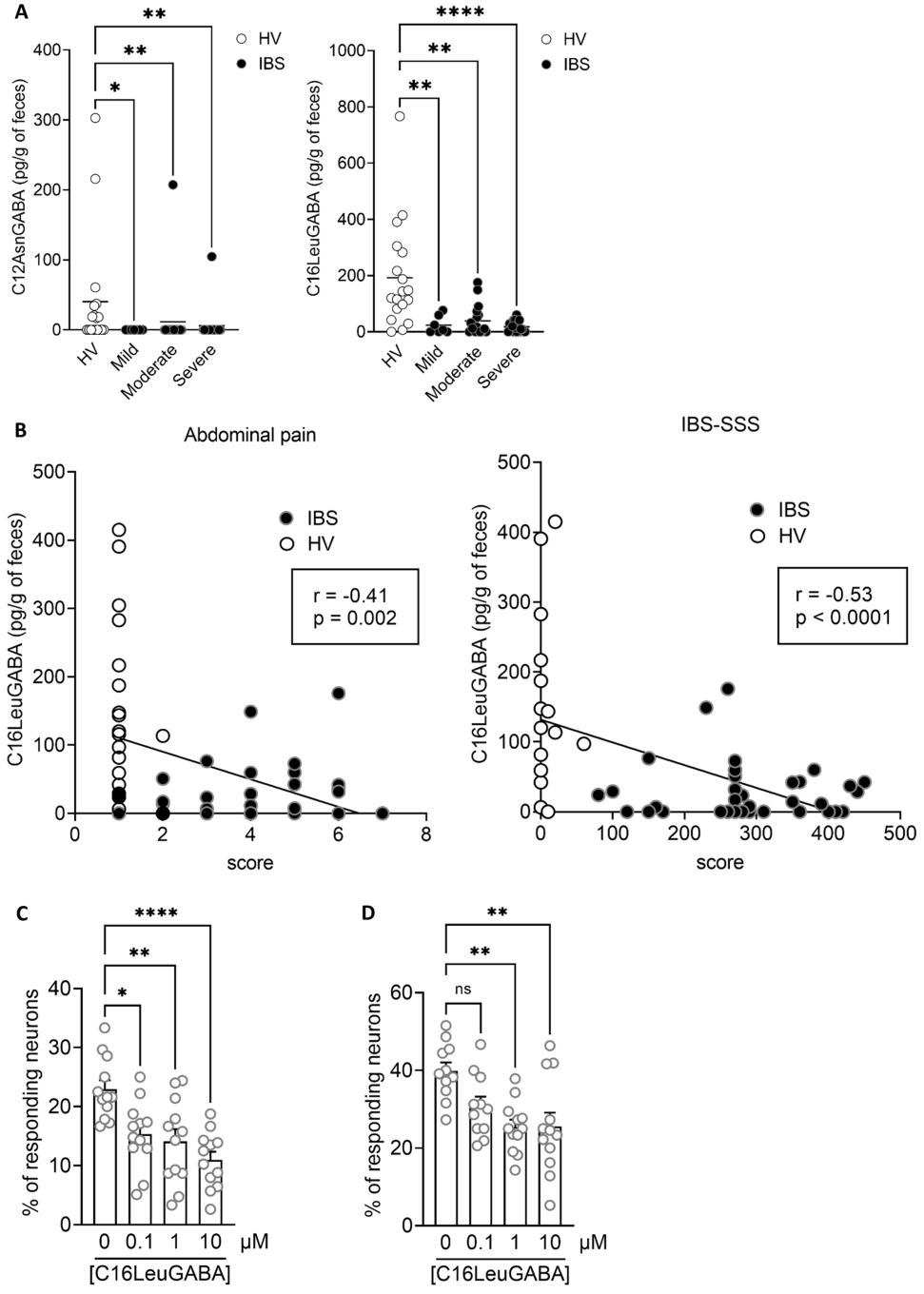

Figure 7 Lipopeptide–GABA concentrations are decreased in the faeces of patients with IBS. (A) 16LeuGABA (left panel) and C12AsnGABA (right panel) concentrations quantified by liquid chromatography–tandem mass spectrometry; in the faeces of HVs (n=18, white) and patients with IBS (black) with an IBS-SSS corresponding to mild (n=7), moderate (n=18) or severe (n=18) IBS. Data are expressed as scatter dot plots with the mean. Statistical analysis was performed using Kruskal-Wallis analysis of variance and subsequent Dunn multiple comparison test. **P<0.01, **P<0.001 significantly different from HVs. (B) Spearman correlations were used to analyse the correlation between the concentration of CL16LeuGABA and abdominal pain score (left panel) or IBS-SSS (right panel) in HVs (white) and patients with IBS (black). P and R values are indicated on each graph. (C) Percentage of responding neurons pretreated with increasing amounts of C16LeuGABA or vehicle (HBSS/MeOH 0.06%, 0 µM) and treated with capsaicin (500 nM) or (D) a mix of GPCR agonists (histamine, serotonin and bradykinin, 10 µM each). Data are represented as mean±SEM; n=4 independent experiments of two to three wells per condition and 20–50 neurons per well. Statistical analysis was performed using Kruskal–Wallis analysis of variance and subsequent Dunn post hoc test. *P<0.05, **P<0.01, ****P<0.0001 significantly different from capsaicin or GPCR mix. GPCR, G protein-coupled receptor; IBS-SSS, IBS Severity Scoring System; ns, not significant; HV, healthy volunteer.

in children.[31 32] In rodents, PS has also been associated with an increase of ASD-like behaviours in adulthood,[33–35] but, in the absence of microbiota analysis, a direct link between PS, *C. clostridioforme* and ASD is still unknown. More studies are needed to decipher the implication of *C. clostridioforme* in IBS, but its correlation with behavioural disorders is indicative of a role in psychological comorbidities such as anxiety and depression.

The decreased abundance of the *Lactobacillus* genera seems to be a universal response to chronic stress as this observation has been made in various chronic stress models, applied either

in adulthood or in early life, and in different species.[24 27 36 37] In humans, studies looking at the correlation between stress in pregnancy and the baby's gut microbiota have also highlighted that infants of stressed mothers present a decreased abundance of *Lactobacillus* in their faeces.[38] However, how chronic stress impacts the *Lactobacillus* population and its duration remain to be determined. Given that we previously showed analgesic properties of C12AsnGABA, a lipopeptide containing GABA in a model of visceral pain,[14] the inverse correlation between *L. murinus/animalis* abundance and visceral sensitivity led us to hypothesise that this bacterium was implicated in the maintenance of normosensitivity by producing analgesic molecules. As expected, *L. murinus* IRSD_2020, in the presence of GABA, produced GABA-containing lipopeptides, such as C16PheGABA, C12AsnGABA, C16GluGABA, C14AsnGABA, C12IleGABA, C14IleGABA and C12AlaGABA, highlighting the redundancy to produce lipopeptides linked to GABA.

GABA production is widely distributed in all three life kingdoms: animals, plants and bacteria. In bacteria, the most studied producers belong to the lactic acid-producing bacteria, a group that includes *Lactobacilli*.[39 40] GABA is synthetisd by a pyridocal-5′-phosphate-dependent enzyme glutamate decarboxylase (EC 4.1.1.15) by irreversible α-decarboxylation of L-glutamate and consumption of one cytoplasmic proton.[41] These enzymes are encoded by *gadB* and *gadC* genes.[42] *L. murinus/animalis* does not possess the enzymes required to produce GABA. Nevertheless, when cultivated in a GABA-enriched medium, this species forms lipopeptides linked to GABA. In vivo GABA could be provided to *L. murinus/animalis* by two other hardly differentiable *Lactobacillus* species that we isolated from the mucus of control but not from PS mice, *L. reuteri* and the *L. johnsonii/gasseri* cluster. In the literature, these two latter species tend to form dual-species biofilm in the gut and are often clustering with *L. murinus/animalis*.[43] *L. reuteri* possesses the GABA production machinery,[43] and the close interactions between these species in the gut could be one of the mechanisms through which *L. murinus/animalis* acquires the GABA to produce lipopeptides containing GABA. Interestingly, we quantified a decrease of C16LeuGABA concentration in the faeces of patients with IBS compared with HVs. C16LeuGABA was not quantifiable in *L. murinus/animalis* or in mouse colon, meaning that in human, this lipopeptide could be produced by other species of lactobacillus or even other species of bacteria. The diversity in lipopeptide composition could be dependent on the culture conditions or on the diet as the leucine is an essential fatty acid, which cannot be produced by the organism. In addition, bacterial environment could also have an impact on lipopeptide synthesis as, for the example, the size of fatty acids in bacteria is dependent on culture conditions and temperature.[44 45] A prospective clinical study unifying microbiota analyses and lipopeptides quantification is needed to identify bacteria implicated in the production of C16LeuGABA in the human gut microbiota. As this GABA–lipopeptide decreased capsaicin-induced and GPCR agonist-induced neuronal activation, the contribution of GABA–lipopeptides to visceral pain could be relevant in patients. Quantification of GABA–lipopeptides in patients would allow identification of patients which could be treated directly by the lipopeptide or by a probiotic supplemented with GABA.

GABA analogues such as gabapentine or pregabalin decrease abdominal pain in patients with IBS, but their serious side effects (hepatotoxicity and neurotoxicity) prevent their chronic use.[46–48] The analgesic properties of GABA lipopeptides, as demonstrated here for C14AsnGABA and C16LeuGABA, show that they could represent a novel therapeutic track to explore in patients with IBS. Our results show that the production of lipopeptides–GABA by commensal bacteria could be one of the mechanisms of communication between the host and its gut microbiota implicated in the upkeep of intestinal homeostasis.

Author affiliations
[1]IRSD, Université de Toulouse-Paul Sabatier, INSERM, INRAe, ENVT, UPS, Toulouse, France
[2]Lipidomic, MetaboHUB-MetaToul, National Infrastructure of Metabolomics and Fluxomics, Toulouse, France
[3]I2MC, Université de Toulouse, Inserm, Université Toulouse III – Paul Sabatier (UPS), Toulouse, France
[4]Institut des Neurosciences Cellulaire et Integrative (INCI), Centre National de la Recherche Scientifique, Université de Strasbourg, Strasbourg, France
[5]INFINITY, Université de Toulouse-Paul Sabatier, INSERM, CNRS, UPS, Toulouse, France
[6]Institut des Biomolécules Max Mousseron (IBMM), UMR 5247, CNRS, Université de Montpellier, ENSCM, Montpellier, France
[7]Service de bactériologie-hygiène, CHU Toulouse, Hôpital Purpan, Toulouse, France
[8]Toxalim (Research Center in Food Toxicology), Toulouse University, INRAE, ENVT, INP-Purpan, UPS, Toulouse, France
[9]Metatoul-AXIOM Platform, MetaboHUB, Toxalim, INRAE, Toulouse, France
[10]Laboratory of Intestinal Neuro-immune Interaction, Translational Research Center for Gastrointestinal Disorders, Department of Chronic Diseases, Metabolism and Ageing, KU Leuven, Leuven, Belgium
[11]Gastroenterology Department, Rouen University Hospital, Rouen, France
[12]Institute for Research and Innovation in Biomedicine, INSERM CIC-CRB 1404, INSERM UMR 1073, Normandy University, Rouen, France
[13]Department of Molecular and Clinical Medicine, Institute of Medicine, Sahlgrenska Academy, University of Gothenburg, Gothenburg, Sweden

Acknowledgements We gratefully acknowledge the animal care facility, Genetoul, anexplo, US006/INSERM, Toulouse, MetaToul (Toulouse metabolomics and fluxomics facilities, www.metatoul.fr) which is part of the French National Infrastructure for Metabolomics and Fluxomics MetaboHUB and the platform Aninfimip, an EquipEx ('Equipement d'Excellence') supported by the French government through the Investments for the Future programme. We acknowledge the technical assistance provided by the personnel of flow cytometry Infinity core facility and the cellular imaging facility of INSERM 1291 connected to the 'Toulouse Réseau Imagerie' network.

Contributors CP, PLF and NC designed the research studies; conducted the experiments; and acquired, analysed the data and wrote the manuscript. SM, GP and MSdesigned the research studies, conducted the experiments, and acquired and analysed the data. AH, BA RM and FA conducted the experiments and acquired and analysed the data. GL, J-PM, PF, SL and AD acquired and analysed the data. MT-F analysed the data. JMG, AG and TD designed and synthesised the lipopeptides. GG, JB-M, AS, EO PB and GD designed the research studies and wrote the manuscript. HH and LD provided patient samples and clinical scores. CM and GB provided patient samples and clinical scores and wrote the manuscript. PLF and NC are responsible for the overall content as guarantor.

Funding Funding from the Agence Nationale de la Recherche (ANR): ANR-18-CE14-0039 for N.C, ANR-20-CE14-0011 for NC & JBM, ANR-17-EURE-022 for EURIDOL Graduate School of Pain, ANR-11-INBS-0010 for Metabohub, ANR-11-EQPX-0003 for the platform Aninfimip. Funding from the Fédération pour la Recherche sur le Cerveau (FRC) FRC20200411001 for AS and NC. AS, PP and GG are supported by Centre National de la Recherche Scientifique. PP and GG received support from CNRS and University of Strasbourg. GG, CP and SM received a scholarship from Ministère de l'Enseignement Supérieur, de la Recherche et de l'Innovation.

Competing interests PP is a senior fellow of the Institut Universitaire de France. CM has been awarded the UEG Research Award 2020 for her stay at The University of Gothenburg and by the FARE Fellowship of the French Gastroenterology Society in 2015.

Patient and public involvement Patients and/or the public were not involved in the design, conduct, reporting or dissemination plans of this research.

Patient consent for publication Not applicable.

Ethics approval This study involves human participants. For French patients, the use of informatics data was declared to the CNIL (number 817.917) and the biological collection was declared to the French Ministry (numbers DC 2016-2637 and AC 2019-3840). Collection of samples from healthy volunteers and patients with IBS in Leuven was approved by the medical ethics committee of the University Hospitals Leuven (B) (S51573). The research was performed according to the Declaration of Helsinki. All patients gave their written informed consent. For animal experiments, all procedures were performed in accordance with the Guide for the

Care and Use of Laboratory Animals of the European Council and were approved by the Animal Care and Ethics Committee of US006/CREFE (CEEA-122; application number APAFIS #16385CE2018080222083660V3).

Provenance and peer review Not commissioned; externally peer reviewed.

Data availability statement All data relevant to the study are included in the article or uploaded as supplementary information.

ORCID iDs
Géraldine Gazzo http://orcid.org/0000-0002-1796-8363
Jean-Paul Motta http://orcid.org/0000-0002-9464-0695
Hind Hussein http://orcid.org/0000-0001-6309-8242
Gilles Dietrich http://orcid.org/0000-0002-2232-1716
Guy Boeckxstaens http://orcid.org/0000-0001-8267-5797
Matteo Serino http://orcid.org/0000-0003-4644-8532
Nicolas Cenac http://orcid.org/0000-0002-1552-7812

REFERENCES

1 Enck P, Aziz Q, Barbara G, *et al*. Irritable bowel syndrome. *Nat Rev Dis Primers* 2016;2:16014.
2 Surdea-Blaga T, Băban A, Dumitrascu DL. Psychosocial determinants of irritable bowel syndrome. *World J Gastroenterol* 2012;18:616.
3 Blanchard EB, Lackner JM, Jaccard J, *et al*. The role of stress in symptom exacerbation among IBS patients. *J Psychosom Res* 2008;64:119–28.
4 Chang L. The role of stress on physiologic responses and clinical symptoms in irritable bowel syndrome. *Gastroenterology* 2011;140:761–5.
5 Caparros-Gonzalez RA, Torre-Luque Adela, Romero-Gonzalez B, *et al*. Stress during pregnancy and the development of diseases in the offspring: a Systematic-Review and meta-analysis. *Midwifery* 2021;97:102939.
6 Olén O, Stephansson O, Backman A-S, *et al*. Pre- and perinatal stress and irritable bowel syndrome in young adults - A nationwide register-based cohort study. *Neurogastroenterol Motil* 2018;30:e13436.
7 Low EXS, Mandhari MNKA, Herndon CC, *et al*. Parental, perinatal, and childhood risk factors for development of irritable bowel syndrome: a systematic review. *J Neurogastroenterol Motil* 2020;26:437–46.
8 Bradford K, Shih W, Videlock EJ, *et al*. Association between early adverse life events and irritable bowel syndrome. *Clin Gastroenterol Hepatol* 2012;10:385–90.
9 Jašarević E, Howard CD, Morrison K, *et al*. The maternal vaginal microbiome partially mediates the effects of prenatal stress on offspring gut and hypothalamus. *Nat Neurosci* 2018;21:1061–71.
10 Tap J, Derrien M, Törnblom H, *et al*. Identification of an intestinal microbiota signature associated with severity of irritable bowel syndrome. *Gastroenterology* 2017;152:111–23.
11 Su T, Liu R, Lee A, *et al*. Altered Intestinal Microbiota with Increased Abundance of *Prevotella* Is Associated with High Risk of Diarrhea-Predominant Irritable Bowel Syndrome. *Gastroenterol Res Pract* 2018;2018:1–9.
12 Lepage P, Leclerc MC, Joossens M, *et al*. A metagenomic insight into our gut's microbiome. *Gut* 2013;62:146–58.
13 HuttenhowerC, GeversD, KnightR, *et al*. Structure, function and diversity of the healthy human microbiome. *Nature* 2012;486:207–14.
14 Pérez-Berezo T, Pujo J, Martin P, *et al*. Identification of an analgesic lipopeptide produced by the probiotic Escherichia coli strain Nissle 1917. *Nat Commun* 2017;8:1314.
15 Hueber A, Gimbert Y, Langevin G, *et al*. Identification of bacterial lipo-amino acids: origin of regenerated fatty acid carboxylate from dissociation of lipo-glutamate anion. *Amino Acids* 2022;54:241–50.
16 Hueber A, Petitfils C, Le Faouder P, *et al*. Discovery and quantification of lipoamino acids in bacteria. *Anal Chim Acta* 2022;1193:339316.
17 Bautzova T, Hockley JRF, Perez-Berezo T, *et al*. 5-oxoETE triggers nociception in constipation-predominant irritable bowel syndrome through Mas-related G protein-coupled receptor D. *Sci Signal* 2018;11:eaal2171.
18 Cenac N, Bautzova T, Le Faouder P, *et al*. Quantification and potential functions of endogenous agonists of transient receptor potential channels in patients with irritable bowel syndrome. *Gastroenterology* 2015;149:433–44.
19 Lacy BE, Mearin F, Chang L, *et al*. Bowel disorders. *Gastroenterology* 2016;150:1393–407.
20 Francis CY, Morris J, Whorwell PJ. The irritable bowel severity scoring system: a simple method of monitoring irritable bowel syndrome and its progress. *Aliment Pharmacol Ther* 1997;11:395–402.
21 Boeckxstaens GE, Drug V, Dumitrascu D, *et al*. Phenotyping of subjects for large scale studies on patients with IBS. *Neurogastroenterol Motil* 2016;28:1134–47.
22 Zheng J, Wittouck S, Salvetti E, *et al*. A taxonomic note on the genus *Lactobacillus*: Description of 23 novel genera, emended description of the genus *Lactobacillus* Beijerinck 1901, and union of *Lactobacillaceae* and *Leuconostocaceae*. *Int J Syst Evol Microbiol* 2020;70:2782–858.
23 Park SH, Itoh K. Species-specific oligonucleotide probes for the detection and identification of *Lactobacillus* isolated from mouse faeces. *J Appl Microbiol* 2005;99:51–7.
24 Golubeva AV, Crampton S, Desbonnet L, *et al*. Prenatal stress-induced alterations in major physiological systems correlate with gut microbiota composition in adulthood. *Psychoneuroendocrinology* 2015;60:58–74.
25 Wang H-J, Xu X, Xie R-H, *et al*. Prenatal maternal stress induces visceral hypersensitivity of adult rat offspring through activation of cystathionine- β -synthase signaling in primary sensory neurons. *Mol Pain* 2018;14:174480691877740.
26 Bernatova I, Puzserova A, Balis P, *et al*. Chronic stress produces persistent increases in plasma corticosterone, reductions in brain and cardiac nitric oxide production, and delayed alterations in endothelial function in young prehypertensive rats. *Front Physiol* 2018;9:1179.
27 Jašarević E, Howard CD, Misic AM, *et al*. Stress during pregnancy alters temporal and spatial dynamics of the maternal and offspring microbiome in a sex-specific manner. *Sci Rep* 2017;7:44182.
28 van Bodegom M, Homberg JR, Henckens MJAG. Modulation of the hypothalamic-pituitary-adrenal axis by early life stress exposure. *Front Cell Neurosci* 2017;11:87.
29 Haas KN, Blanchard JL. Reclassification of the *Clostridium clostridioforme* and *Clostridium sphenoides* clades as *Enterocloster* gen. nov. and *Lacrimispora* gen. nov., including reclassification of 15 taxa. *Int J Syst Evol Microbiol* 2020;70:23–34.
30 Finegold SM, Song Y, Liu C, *et al*. Clostridium clostridioforme: a mixture of three clinically important species. *Eur J Clin Microbiol Infect Dis* 2005;24:319–24.
31 Finegold SM, Molitoris D, Song Y, *et al*. Gastrointestinal microflora studies in late-onset autism. *Clin Infect Dis* 2002;35:S6–16.
32 Song Y, Liu C, Finegold SM. Real-Time PCR quantitation of clostridia in feces of autistic children. *Appl Environ Microbiol* 2004;70:6459–65.
33 Weinstock M. Prenatal stressors in rodents: effects on behavior. *Neurobiol Stress* 2017;6:3–13.
34 Kinney DK, Munir KM, Crowley DJ, *et al*. Prenatal stress and risk for autism. *Neurosci Biobehav Rev* 2008;32:1519–32.
35 Weinstock M. The long-term behavioural consequences of prenatal stress. *Neurosci Biobehav Rev* 2008;32:1073–86.
36 Hantsoo L, Zemel BS. Stress gets into the belly: early life stress and the gut microbiome. *Behav Brain Res* 2021;414:113474.
37 Mackos AR, Varaljay VA, Maltz R, *et al*. Role of the intestinal microbiota in host responses to stressor exposure. *Int Rev Neurobiol* 2016;131:1–19.
38 Zijlmans MAC, Korpela K, Riksen-Walraven JM, *et al*. Maternal prenatal stress is associated with the infant intestinal microbiota. *Psychoneuroendocrinology* 2015;53:233–45.
39 Dhakal R, Bajpai VK, Baek K-H. Production of gaba (γ - Aminobutyric acid) by microorganisms: a review. *Braz J Microbiol* 2012;43:1230–41.
40 Seok J-H, Park K-B, Kim Y-H. Production and characterization of kimchi with enhanced levels of γ-aminobutyric acid;7.
41 Ueno H. Enzymatic and structural aspects on glutamate decarboxylase. *J Mol Catal B Enzym* 2000;10:67–79.
42 Ma D, Lu P, Yan C, *et al*. Structure and mechanism of a glutamate-GABA antiporter. *Nature* 2012;483:632–6.
43 Lin XB, Wang T, Stothard P, *et al*. The evolution of ecological facilitation within mixed-species biofilms in the mouse gastrointestinal tract. *Isme J* 2018;12:2770–84.
44 Núñez-Cardona MT. Influence of culture conditions on the fatty acid composition of green and purple photosynthetic sulphure bacteria. *IntechOpen* 2014.
45 Suutari M, Laakso S. Microbial fatty acids and thermal adaptation. *Crit Rev Microbiol* 1994;20:285–328.
46 Cui Y, Miao K, Niyaphorn S, *et al*. Production of gamma-aminobutyric acid from lactic acid bacteria: a systematic review. *Int J Mol Sci* 2020;21:995.
47 Zhang M-M, Liu S-B, Chen T, *et al*. Effects of NB001 and gabapentin on irritable bowel syndrome-induced behavioral anxiety and spontaneous pain. *Mol Brain* 2014;7:47.
48 Saito YA, Almazar AE, Tilkes KE, *et al*. Randomised clinical trial: pregabalin vs placebo for irritable bowel syndrome. *Aliment Pharmacol Ther* 2019;49:389–97.

Identification of bacterial lipopeptides as key players in IBS

Camille Petitfils[1]*, Sarah Maurel[1]*, Gaëlle Payros[1], Amandine Hueber[2,3], Bahija Agaiz[1], Geraldine Gazzo[4], Rémi Marrocco[5], Frédéric Auvray[1], Geoffrey Langevin[6], Jean-Paul Motta[1], Pauline Floch[1,7], Marie Tremblay-Franco[8,9], Jean-Marie Galano[6], Alexandre Guy[6], Thierry Durand[6], Simon Lachambre[5], Anaëlle Durbec[2,3], Hind Hussein[10], Lisse Decraecker[10], Justine Bertrand Michel[2,3], Abdelhadi Saoudi[5], Eric Oswald[1,7], Pierrick Poisbeau[4], Gilles Dietrich[1], Chloé Melchior[11], Guy Boeckxstaens[10], Matteo Serino[1], Pauline le Faouder[2,3#], Nicolas Cenac[1#].

[1] IRSD, Université de Toulouse-Paul Sabatier, INSERM, INRAe, ENVT, UPS, Toulouse, France
[2] MetaboHUB-MetaToul, National Infrastructure of Metabolomics and Fluxomics, Toulouse, France
[3] I2MC, Université de Toulouse, Inserm, Université Toulouse III – Paul Sabatier (UPS), Toulouse, France.
[4] Centre National de la Recherche Scientifique, Université de Strasbourg, Institut des Neurosciences Cellulaire et Integrative (INCI), Strasbourg, France.
[5] INFINITY, Université de Toulouse-Paul Sabatier, INSERM, CNRS, UPS, 31000 Toulouse, France
[6] Institut des Biomolécules Max Mousseron (IBMM), UMR 5247, CNRS, Université de Montpellier, ENSCM, Montpellier, France
[7] CHU Toulouse, Hôpital Purpan, Service de bactériologie-hygiène, Toulouse, France
[8] Toxalim (Research Center in Food Toxicology), Toulouse University, INRAE, ENVT, INP-Purpan, UPS, F-31027 Toulouse, France.
[9] Metatoul-AXIOM Platform, MetaboHUB, Toxalim, INRAE, F-31027 Toulouse, France.
[10]Laboratory of Intestinal Neuro-immune Interaction, Translational Research Center for Gastrointestinal Disorders, Department of Chronic Diseases, Metabolism and Ageing, KU Leuven, Leuven, Belgium.
[11]Rouen University Hospital, Gastroenterology Department and INSERM CIC-CRB 1404, and INSERM UMR 1073, Institute for Research and Innovation in Biomedicine, Normandy University, Rouen, France. Current address: Department of Molecular and Clinical Medicine, Institute of Medicine, Sahlgrenska Academy, University of Gothenburg, Gothenburg, Sweden.

* Joint first author
# Joint last author

Index

Supplementary methods

Colorectal distension

Nickel-chrome electrodes were implanted in the abdominal external oblique musculature of anesthetized mice in order to detect EMG activity as previously described [1]. CRD was performed 3 days post-surgery by inserting a distension catheter (Fogarty catheter for arterial embolectomy, 4 F; Edwards Lifesciences, Nijmegen, Netherlands) into the colon at 5 mm from the anus. The balloon was progressively inflated in a stepwise of 15mmHg (from 0 to 60mmHg) performing 10s distension for each pressure and with resting intervals of 5min (n=14-19 mice/group, 3 independent experiments). In a second set of experiments, mice submitted to stress (n=15 per group, 2 independent experiments) were treated with a 100µL intracolonic injection of C14snGABA (10µM) or its vehicle (EtOH 40%) 30min before CRD. The results were expressed as the area under the curve from 15 to 60mmHg.

Permeability and macro and microscopic scores

To determine paracellular permeability, mice were gavaged with dextran 4kDa-FITC (25mM; Sigma, St. Quentin Fallavier, France). Four hours after, mice were sacrificed. Blood was collected for FITC quantification in the serum and colons were removed. Length and thickness were measured and macroscopic colonic tissue damages were scored from 0 to 3 for the intensity of adhesion and strictures, from 0 to 2 for the intensity of edema, erythema, ulceration and diarrhea and from 0 to 1 (absent or present) for the mucus, hemorrhage and fecal blood; the maximal score being 17. For histological examination, a piece of colon located at 2cm proximal to the anus was resected, fixed in 10% phosphate buffered formalin, embedded in paraffin, sectioned, and stained with hematoxylin–eosin. Slides were examined and graded for cellular infiltration, mucosal architecture alteration and submucosal oedema from 0 to 3 (absent, mild, moderate and severe) and vasculitis, muscular thickening, crypt abscess and goblet cell depletion from 0 to 1 (absent or present); the maximal score being 13.

Real time PCR analysis

Colon biopsies were crushed in 500µL of Trizol (Invitrogen, Thermofisher scientific, Saclay, France) in Precellys lysing kit tubes (Bertin Technologies, Montigny le Bretonneux, France) placed in a Precellys (2823g, 30 seconds twice; Bertin Technologies). After addition of

chloroform and centrifugation (15 minutes, 11292 g at 4°C), the supernatant containing the RNA was removed. Ethanol 70% (vol/vol) was added and the contents were placed in columns (GenElute® mammalian total RNA miniprep kit, Sigma Aldrich). The RNA was extracted according to the manufacturer recommendations. Subsequently the RNA was dosed in a nanodrop (implenGmbH, Dominique Dutscher, Issy-les-Moulineaux, France). RNA (3µg) preparations from colon of mice were used for the total RNA reverse-transcription with Moloney murine leukemia virus reverse transcriptase (Fisher Scientific) using random hexamers (Fisher Scientific) for priming. Transcripts encoding Hypoxanthine phosphoribosyl transferase (Hprt), Trefoil factor 3 (Tff3), Mucin 2 (Muc2), Occludin (Ocln), Zonula occludens-1 (Tjp1), Regenerating islet-derived 3 gamma (Reg3γ), Matrilysin (Mmp7), Tumor necrosis factor alpha (Tnfα), Chemokine (C-Cmotif) ligand 5 (Ccl5), Transforming growth factor beta (Tgfβ), Interleukin 6 (Il6), Interleukine 1 beta (Il1β), Nuclear factor kappa B (Nfκb), Chemokine (C-X-C motif) 2 ligand Cxcl2, Lipoxygenase 15 (Alox15), Lipoxygenase 5 (Alox5), Lipoxygenase 12 (Alox12), Cyclooxygenase 1 (Ptgs1), Cyclooxygenase 2 (Ptgs2), Pro-enkephaline (Penk), Interferon gamma (Ifnγ), Peroxysome proliferator-Activated Receptor(PPARα), Acyl-CoA Thioesterase 12 (Acot12), Angiopoietine like 4 (Angptl4), Cluster of differenciation 36 (CD36), Aryl hydrocarbon receptor (Ahr), glucocorticoid receptor (Nr3C1) and soluble epoxy hydrolase (Ephx2), were quantified by real-time PCR using specific forward and reverse primers (**Table S3**), the kit Takyon SYBR 2X MasterMix blue dTTP (Eurogentec) and the LightCycler480II (Roche Diagnostics, Meylan, France). Hierarchical clustering was performed, and heat maps were obtained with R (www.rproject.org). Gene expressions were transformed to z scores and clustered based on 1− Pearson correlation coefficient as distance and the Ward algorithm as agglomeration criterion.

Liquid chromatography/tandem mass spectrometry (LC-MS/MS) measurements

PUFA metabolites were quantified from mice colons by mass spectrometry after lipid extraction as previously described [2]. After the addition of 500µL of PBS, and 5µL deuterated Internal Standard (IS) mixture (5-HETEd8, LxA4d4 and LtB4d4), the colons were crushed in lysing MatrixA tubes in a precellys (Bertin Technologies). After two crush cycles (6.5 ms−1, 30s), 10µL of suspensions were withdrawn for protein quantification and 0.3mL of cold methanol (MeOH) were added. The samples were centrifuged at 1016 × g for 15min (4°C) and the resulting supernatants were submitted to solid phase extraction of lipids using HLB plate

(OASIS® HLB 30 mg, 96-well plate, Waters, Saint-Quentin-en-Yvelines, France). Briefly, plates were conditioned with 500µL MeOH and 500µL H2O/MeOH (90:10, v/v). Samples were loaded at a flow rate of about one drop per 2s and, after complete loading, columns were washed with 500µL H2O/MeOH (90:10, v/v). The phase was thereafter dried under aspiration and lipids were eluted with 750µL MeOH. Solvent was evaporated under N2 and samples were resuspended with 140µL MeOH and transferred into a vial (Macherey-Nagel, Hoerdt, France). Finally, the 140µL of methanol were evaporated and our sample resuspended with 10µL of methanol for liquid chromatography/mass spectrometry analysis. 6-keto-prostaglandin F1 alpha (6k$PGF_{1\alpha}$), thromboxane B2 (TxB2), Prostaglandin E2 (PGE_2), 8-iso Prostaglandin A2 (8-isoPGA_2), Prostaglandin E3 (PGE_3), 15-Deoxy-Δ12,14-prostaglandin J2 (15d-PGJ_2), Prostaglandin D2 (PGD_2), Lipoxin A4 (LxA4), LxB4, Resolvin D1 (RvD1), Resolvin D2 (RvD2), Resolvin D5 (RvD5), 7-Maresin 1 (7-Mar1), Leukotriene B4 (LtB4), Leukotriene B5 (LtB5), Protectin Dx (PDx), 18-hydroxyeicosapentaenoic (18-HEPE), 5,6-dihydroxyeicosatetraenoic acid (5,6-DiHETE), 9-hydroxyoctadecadienoic acid (9-HODE), 13-hydroxyoctadecadienoic acid (13-HODE), 15-hydroxyeicosatetraenoic acid (15-HETE), 12-hydroxyeicosatetraenoic acid (12-HETE), 8-hydroxyeicosatetraenoic acid (8-HETE), 5-hydroxyeicosatetraenoic acid (5-HETE), 17-hydroxydocosahexaenoic acid (17-HDoHE), 14-hydroxydocosahexaenoic acid (14-HDoHE), 14,15-epoxyeicosatrienoic acid (14,15-EET), 11,12-epoxyeicosatrienoic acid (11,12-EET), 8,9-epoxyeicosatrienoic acid (8,9-EET), 5,6-epoxyeicosatrienoic acid (5,6-EET), 5-oxoeicosatetraenoic acid (5-oxoETE), Prostaglandin F2α, ($PGF_{2\alpha}$), 13-Hydroxyoctadecadienoic acid (13oxoODE), 9-hydroxyoctadecadienoic acid (9oxoODE), 10-hydroxyoctadecadienoic acid (10-HODE), 9,10-dihydroxy-12-octadecenoic acid (9,10-DiHOME), 12,13-dihydroxy-12-octadecenoic acid (12,13-DiHOME), 9-hydroxy-10,12,15-octadecatrienoic acid (9-HOTrE), 13-hydroxy-9,11,15-octadecatrienoic acid (13-HOTrE), 9,10,13-trihydroxy-11-octadecenoic acid (10-TriHOME) and 9,12,13-trihydroxy-11E-octadecenoic acid (12-TriHOME) were quantified in mouse colons. To simultaneously separate 42 lipids of interest and three deuterated internal standards (5-HETEd8, LxA4d4 and LtB4d4), LC-MS/MS analysis was performed on an ultrahigh-performance liquid chromatography system (UHPLC; Agilent LC1290 Infinity) coupled to an Agilent 6460 triple quadrupole MS (Agilent Technologies) equipped with electrospray ionization operating in negative mode. Reverse-phase UHPLC was performed using a Zorbax SB-C18 column (Agilent Technologies) with a gradient elution. The mobile phases consisted of water, acetonitrile (ACN), and formic acid (FA) [75:25:0.1 (v/v/v)] (solution A) and ACN and FA

[100:0.1 (v/v)] (solution B). The linear gradient was as follows: 0% solution B at 0 min, 85% solution B at 8.5min, 100% solution B at 9.5min, 100% solution B at 10.5min, and 0% solution B at 12 min. The flow rate was 0.4ml/min. The autosampler was set at 5°C, and the injection volume was 5µL. Data were acquired in multiple reaction monitoring (MRM) mode with optimized conditions. Peak detection, integration, and quantitative analysis were performed with MassHunter Quantitative analysis software (Agilent Technologies). Blank samples were evaluated, and their injection showed no interference (no peak detected), during the analysis. Hierarchical clustering was performed, and heat maps were obtained with R (www.rproject.org). PGJ2, RVD1, RVD2, RVD5, 7Mar1, 5,6-DiHETE were not detected in our samples. PUFA metabolite amounts were transformed to z scores and clustered based on 1− Pearson correlation coefficient as distance and the Ward algorithm as agglomeration criterion.

Dosage of the corticosterone

Mice were anesthetized with ketamine/xylasine and submandibular blood was collected into tubes and centrifuged (15min, 8000rpm) to separate the serum. Serum samples were stored at -80°C until analysis. Corticosterone levels were determined using the corticosterone AlphaLISA detection kit (PerkinElmer, AL3020C) following manufacturer's instructions. The volumes of all reagents were adjusted for the use 5µl of serum or standard. The serum samples were diluted 1:5 into 1X diluent. The corticosterone concentrations in serum samples were expressed in ng/ml. (n=8 to 10 mice/group).

Phenotypic analysis of mesenteric lymph node cells

11 weeks old controls or prenatally stressed mice were euthanized and their mesenteric lymph node cells were stained with conjugated antibodies for flow cytometry analysis. The monoclonal antibodies (mAbs) used for flow cytometry were as follows: anti-TCRαβ-BV711(H57-597), anti-CD4-BV786, (GK1.5), anti-CD8α-A700 (53-6.7), anti-CD44-Percep5.5 (IM7) and anti-CD62L-APC (MEL-14), and with a viability dye (APC-H7) to exclude dead cells. We used the Foxp3/transcription factor permeabilization kit according to the manufacturer's instructions (e-Biosciences) to fix and permeabilize the cells prior to intracellular staining with anti-Foxp3 labelled antibody (Foxp3-BV421 (FJK-16s)). The fluorescently conjugated antibodies were purchased from e-Biosciences, BD Biosciences, and Biolegend. Data were collected on LSR-Fortessa cytometer (BD Biosciences) and analyzed using the FlowJo software.

Fecal bacterial DNA extraction

Feces were collected and frozen at -80°C until use. 15 feces/ group chosen from 3 independent experiments. Metagenomic DNA was extracted from the feces using a QIAamp DNA Stool Mini Kit (Qiagen, Hilden,Germany) according to the manufacturer's instructions. Quickly, the feces were crushed in the inhibitex buffer at (6.5 ms−1, 3x30 s), placed at 95°C and then were centrifuged 2min, at 16 000g, at room temperature to pellet the stool particles. 200µL of the supernatant were added to 15µL of proteinase K and AL buffer and incubated 10min at 70°C. 200µL of EtOH were added and the samples were added in the spin columns and centrifuged at 16 000g at room temperature for 1 minute. The supernatant was removed and 500µL of washing buffer 1 was added. After centrifugation at 16 000g at room temperature for 1 minute, the supernatant was removed and 500µL of washing buffer 2 was added. After centrifugation at 16 000g at room temperature for 3 minutes, the supernatant was removed and 50µL of the elution buffer was added. Finally, the samples were centrifuged for 1 minute at 16 000g at room temperature and the DNA was collected. The DNA was then quantified using a Nanodrop.

Taxonomic and predicted functional analysis of gut microbiota

Total DNA was extracted from freshly-collected snap-frozen feces as already described [3]. The 16S rRNA gene V3-V4 regions were targeted by the 357wf-785R primers and analyzed by MiSeq at RTLGenomics (http://rtlgenomics.com/, Texas, USA). An average of 29795 sequences was generated per sample. A complete description of the applied bioinformatic filters is available (http://www.rtlgenomics.com/docs/Data_Analysis_Methodology.pdf). LDA scores were drawn by the Huttenhower Galaxy web application (http://huttenhower.sph.harvard.edu/galaxy/) via the LEfSe algorithm [4]. The predictive functional analysis (gut microbiome) of gut microbiota was performed via PICRUSt [5]. Diversity indices were calculated with the software PAST4 [6].

Biofilm

For fluorescent *in situ* hybridization, a specimen of colon with a feces was resected, fixed in carnoy (60% MeOH, 30% chloroform, 10% acetic acid), embedded in paraffin, sectioned, and labelled with the universal bacterial 16 S fluorescent rRNA probe EUB338-Cy3, 5'-GCTGCCTCCCGTAGGAGT-3'Cy5, Eurofins) at 10µL/mL, wheat germ agglutinin-FITC 1/1000

(Sigma-Aldrich L4895) was used to stain the polysaccharide-rich mucus layer, and the epithelial cell nucleus was stained with DAPI (ProLong Gold antifade reagent with DAPI, Invitrogen P36935). Bacterial penetration into the mucus was measured by image processing on Fiji by quantifying the number of 16S RNA labelled pixel between the edge of the lumen to the edge of the epithelium (n=12 mice/group; 4 images/mice, 2 independent experiments). The mucus zone was manually traced, and an arbitrary distance was assigned to each pixel from the middle to the epithelial cells border. Cyanine 5 labelled pixels in this zone were assigned to their corresponding distance. The distance of each pixel in regard to the luminal compartment and the number of labeled pixels between the edge of the lumen to middle of the mucus (Apical) and between the middle of the mucus to the edge of the epithelium (Basal) were quantified.

Identification of colonic mouse bacteria

Ligilactobacillus murinus strain IRSD_2020, *Limosilactobacillus reuteri* and *Lactobacillus johnsonii/gasseri* were isolated from mouse intestinal mucosa on *Lactobacillus* selection agar (BD Diagnostic, Le Pont de Claix, France), and identified by matrix-assisted laser desorption/ionisation time-of-flight mass spectrometry (Microflex LT MALDI-TOF MS, Bruker Daltonik GmbH, Germany). Whole genome sequencing of *Ligilactobacillus murinus* strain IRSD_2020 has been performed as well as the quantification of this strain and of *Ligilactobacillus animalis* by Taqman® real-time PCR. *Ligilactobacillus murinus* strain IRSD_2020 was cultured and GABA-containing lipopeptides quantified.

Whole genome sequencing of *Ligilactobacillus murinus* IRSD_2020

Genomic DNA from *L. murinus* IRSD_2020 and *L. animalis* DSMZ 20602 were purified from 200 µL overnight cultures with MagNA Pure 96 DNA and Viral NA Small Volume Kit (Roche Diagnostics France SAS, Meylan, France) and sequenced in 2x150 bp paired-end by illumina® NextSeq500 (IntegraGen SA, Evry, France) with an 80x coverage. Libraries were obtained by enzymatic fragmentation using a 5X WGS Fragmentation mix kit (Enzymatics Inc., Beverly, MA, USA). The sequence data generated were deposited in the NCBI BioProject database (https://www.ncbi.nlm.nih.gov/bioproject/) under the accession the number PRJNA770189.

Quantification of *Ligilactobacillus murinus* IRSD_2020 and *Ligilactobacillus animalis* using TaqMan® real-time PCR

Primers and probes included in the real-time PCR assay targeting *L. murinus* were selected in an 834 bp-long open reading frame (ORF) whose sequence was retrieved from *L. murinus* IRSD_2020 genome and was found with >99% similarity in other *L. murinus* strains and with <77% similarity in *Streptococcus suis* (**Figure S1**). Primers and probes included in the real-time PCR assay targeting *L. animalis* were selected in the 16S-23S internal transcribed spacer (ITS) region. All the primers and probes (**Table S4**) were designed with TaqMan® Primer and Probes Design Tool (Genescript, Leiden, the Netherlands) and purchased from Eurofins Genomics (Germany). Detection was achieved with LightCycler480II (Roche Diagnostics, Meylan, France) real-time PCR system according to the manufacturer's instructions. TaqMan® qPCRs were performed in 10µL reactions containing: 1X iQ Supermix (Biorad), 0.3µM each primer, 0.2µM probe, 2µl purified DNA diluted 1:10 and nuclease-free water. The bacterial DNA qPCR was performed using the following conditions: 95°C for 3 min, followed by 45 cycles consisting of 95°C for 15 s and 60° for 60 s. Duplicate reactions were run for all samples. The cycle threshold of each sample was then compared with a DNA standard. DNA standard was obtained by purification of *Ligilactobacillus* genomic DNA from the 10ml pellet of overnight culture using the QIAamp Fast DNA Stool Mini Kit (Qiagen, Hilden, Germany). Ten-fold serial dilutions of DNA standard were used to generate a standard curve. The data was expressed as *Ligilactobacillus* copies per ng of isolated DNA.

Bacterial culture

L. murinus IRSD_2020 was grown on Lactobacilli MRS broth (Difco, Fisher scientific SAS, Illkirch, France) – agar plates supplemented with cysteine chloride monohydrate 0.5g.L-1. After 24 hours of incubation at 37°C, 3 colonies were seeded in 30 mL of MRS broth supplemented with cysteine chloride monohydrate 0.5g.L-1 (Merck–Sigma Aldrich, St. Quentin Fallavier, France) and incubated overnight at 37°C. Cultures have been performed with or without GABA (8 mg/mL; Sigma A2129, St. Quentin Fallavier, France) in the medium. All the culture steps have been performed in a hypoxic environment ensured by using a Whitley H35hypoxystation (don Whitley scientific, Bingley, United Kingdom) and all the incubations were done in an anaeropack jar (Fisher scientific SAS, Illkirch, France) with an

anaeroGen sachet (Fisher scientific SAS, Illkirch, France) to ensure an anaerobic environment. Lipopeptides containing GABA were quantified in these bacteria.

Bacterial lipopeptide quantification

To quantify bacterial lipopeptides, mass-spectrometry method has been adapted from the C12AsnGABA quantification method previously described [7] following our previous manuscript on the mass-spectrometry analyses of aminolipids and lipopeptides [8], [9]. For the extraction, 500µL of Tris buffer (pH=9), 1mL of MeOH and 5µL of IS *C16AsnGABA were added to the bacterial pellets or colon samples and crushed with a Fast Prep instrument (MP Biomedicals), using two cycles (6,5m.s-1, 30s). For the human feces, 300 mg of feces were crushed in 500µL of Tris buffer (pH=9) and 1mL of MeOH as described above. In 1/3 of the extract (500 µL), 5µL of IS *C16AsnGABA and 1 mL of Tris/MeOH were added. Ten µL of suspension were withdraw for protein quantification with Biorad assays, then, 6.6mL of water were added to the homogenate. Samples were centrifuged at 1016 x g for 15min (4°C) and the supernatants submitted to SPE using HLB plates (HLB, 30mg, Waters). Plates were conditioned with 750µL ethyl acetate, 750µL MeOH and 750µL H2O:MeOH (90:10; v/v). Samples were loaded at a flow rate of one drop per 2s and SPE plates washed using 1mL H2O:MeOH (90:10; v/v) followed by 1mL heptane. Lipopeptides were eluted using 1mL AcN, 1mL MeOH and 1mL AcOEt. Eluent were carefully removed from the plate, and transferred to a Pyrex tube, dried under nitrogen gas and reconstituted in 10µL MeOH for LC-QqQ (ou LC-LRMS) analysis. Extract was stored at -20°C before LC-MS analysis. High-performance liquid chromatography system was a Shimadzu Mikros LC system, equipped with a thermostated autosampler SIL-30AC, a rack changer II, a Nexera Mikros binary pump, a degasser on-line DGU-20A3R and a LTO-Mikros column oven. The analytical column was a CSH C18 column Waters (1 x 100mm; 2,7µm) and was maintained at 40°C. The mobile phases consisted of water:FA (99.9:0.1; v/v) (A) and acetonitrile:FA (99.9:0.1, v/v) (B). Flow rate was 0.1mL.min-1. The multi-step gradient starts with 30% B at 0 min, 80% B at 13min, 100% B at 13.5min, 100% B at 16 min, and at 16.5 min 30% B until 18min. The chromatography system was coupled online to a triple quadrupole mass spectrometer Shimadzu 8060 equipped with a ESI source in negative mode and was optimized as follow: nebulizer: 2 L.min-1; desolvation line: 250°C; heating-block: 450°C, heating gaz flow: 10L.min-1, and no drying gas was used. Argon gas (purity, >99.9995%) was used for collision-induced dissociation (CID). For each metabolite the

MRM transition (**Table S5**) was optimized on the pure standard to get the best selectivity and the best sensitivity with a qualitative and a quantitative transition and was programmed to monitor a 2min-window (expected chromatographic retention time ± 1min). The dwelltime were optimized for each compound and were set between 15 and 100msec. Peak detection, integration, and quantitative analysis were performed with LabSolution software (Version 5.99 SP2), Shimadzu.

Calcium imaging of sensory neurons

Mouse dorsal root ganglia were dissociated as previously described [10]. After 48h of culture, cells were incubated with HBSS containing 20mM HEPES, 1mM fluo-4 acetoxymethyl (AM) and 20% pluronic F-127 for 30min at 37ºC plus 30min in the dark at RT. The plates were then washed with HBSS and 140µl of HBSS were added to each well. Neurons were pre-treated with C16LeuGABA (0.1, 1, and 10 µM), or vehicle (HBSS/MeOH 0.06%) for 5 min and then were stimulated with either capsaicin or the mix of GPCR agonists. Live cell imaging of calcium was carried out on an automated inverted microscope (Axio Observer, Zeiss, SAS France) with a x10 objective (NA 0.45). Images were acquired using the Zen imaging software (3.1 Blue Edition) and a kinetic of 85 recordings (one per second) was performed. The first ten images were used to determine the baseline and, from 10 to 60 sec, neurons were exposed to either a mix of GPCR agonists (histamine, bradykinin, serotonin, 10 µM), capsaicin (500 nM) or vehicle (HBSS). After 60 seconds, neurons were treated with KCl (50 mM) in order to discriminate neurons from glial cells. The ImageJ software was used to perform the analysis of calcium flux.

Statistical analysis

To perform a multivariate analysis of our cohort, the data obtained from 56 mice (4 groups with 14/group) from 3 different experiments were used to create a matrix including different variables: gene expression, PUFA quantification, VMR to colorectal distension, faecal bacteria abundance from the 16S RNA sequencing, and colon thickness. Principal Component Analysis (PCA) were performed to detect outliers and intrinsic clusters. Then PLS-DA was applied to study the relationship between prenatal stress exposure and variables described above. From this analysis, discriminant variables (with a value of Variance Importance in the Projection, VIP, > 1.0) were selected. Wilcoxon test with FDR correction was applied on

selected variables. PCA, PLS-DA and Wilcoxon test were done using the Galaxy Workflow 4 metabolomics (W4m) instance [11], [12]. Correlations were performed by Spearman test.

Data are presented as means ± standard error of the mean (SEM). Analyses were performed using GraphPad Prism 9.0 software (GraphPad, San Diego, CA). Due to the small sample size and scoring, comparisons between groups were mainly performed by Mann-Whitney non-parametric test. Multiple comparisons within groups were performed by Kruskal-Wallis test, followed by Dunn's post-test. Parametric two-way Anova was used when data were linearly distributed and followed by Bonferroni posthoc test. Statistical significance was set at $P < 0.05$.

Supplementary Table

Supplementary Table S1 PUFA metabolites quantification. Concentration of PUFA metabolites (pg/mg of proteins) in colons of control female (F-CTRL), prenatal stress female (F-PS), control male (M-CTRL) and prenatal stress male (M-PS) mice. Data are expressed as mean ± SEM. Statistical analysis was performed independently for each sex using a Mann-Whitney test. * P<0.05 compared to M-CTRL group.

	Mean ± SEM F-CTRL	**Mean ± SEM F-PS**	**Mean ± SEM M-CTRL**	**Mean ± SEM M-PS**
6kPGF$_{1\alpha}$	84094 ± 11155	96460 ± 18129	102285 ± 15010	83319 ± 10955
TxB2	14186 ± 2248	14363 ± 2054	14363 ± 2249	12422 ± 1552
PGE$_3$	119 ± 809,1	1088 ± 872,1	1043 ± 638,4	1124 ± 55,1
12-TriHOME	7403 ± 3675	6269 ± 4019	10106 ± 5272	9080 ± 7630
PGF$_{2\alpha}$	39315 ± 22747	38106 ± 30182	38567 ± 20861	34640 ± 21751
10-TriHOME	7273 ± 1151	7119 ± 1566	9635 ± 1476	10005 ± 2792
PGE$_2$	81692 ± 13047	81306 ± 14619	73924 ± 10831	67333 ± 9001
PGD$_2$	41575 ± 6777	47094 ± 10117	45921 ± 7468	35403 ± 5002
LxA4	299.6 ± 51.17	284.3 ± 64.08	451.7 ± 68.48	235 ± 41.8*
8isoPGA$_2$	3722 ± 813.1	3405 ± 635.5	2630 ± 553.5	2493 ± 497.6
PDx	63.35 ± 12.37	74.99 ± 16.27	44.32 ± 8.56	36.82 ± 7.55
LTB4	113.4 ± 8.87	128.8 ± 23.45	163.2 ± 46.16	77.65 ± 9.58
12,13-DiHOME	3201 ± 781.4	2712 ± 416.4	2846 ± 324.9	2315 ± 216.5
9,10-DiHOME	602.9 ± 83.68	672.1 ± 113.9	746.7 ± 86.87	576.8 ± 64.65
LTB5	12.32 ± 4.34	8.33 ± 2.95	18.97 ± 4.42	17.52 ± 5.56
9-HOTrE	252.2 ± 52.88	188.4 ± 45.42	339.9 ± 78.27	212.6 ± 48.24
18-HEPE	410.1 ± 75.52	424.5 ± 96.65	649.7 ± 105.2	417.2 ± 86.42
13-HOTrE	241.6 ± 37.01	191.1 ± 36.55	320.3 ± 62.67	305.7 ± 65.08
15-dPGJ$_2$	82.09 ± 18.78	98.98 ± 23.00	70.59 ± 15.24	51.02 ± 8.75
10-HODE	190.3 ± 22.19	223.8 ± 41.89	230.5 ± 22.65	158.4 ± 20.65*
13-HODE	96459 ± 10779	106878 ± 20588	98568 ± 10658	80067 ± 10688
9-HODE	61730 ± 8921	75650 ± 16158	61870 ± 8096	51689 ± 7987
15-HETE	34319 ± 5276	41162 ± 8370	37463 ± 5563	26467 ± 4157

17-HDoHE	11854 ± 1707	13107 ± 3004	9557 ± 1285	7839 ± 1297
13-oxoODE	12419 ± 1454	12511 ± 2367	14612 ± 2094	10072 ± 1406
14-HDoHE	8166 ± 1339	9148 ± 2303	7357 ± 1150	5853 ± 1105
8-HETE	1099 ± 162.9	1349 ± 281.1	1380 ± 222.1	834.9 ± 138.8*
12-HETE	34723 ± 6109	41615 ± 9584	39692 ± 8183	26444 ± 4933
9-oxoODE	12085 ± 1485	11803 ± 1944	13002 ± 1591	9445 ± 905.4
5-HETE	10863 ± 1769	11411 ± 2329	14354 ± 2112	8022 ± 1291*
14,15-EET	61.07 ± 9.75	104.0 ± 16.97	135.0 ± 16.54	71.73 ± 9.02*
5-oxoETE	4592 ± 681.1	5792 ± 1210	8173 ± 1256	4137 ± 717.6*
11,12-EET	147.2 ± 24.94	192.0 ± 44.51	202.0 ± 33.52	94.37 ± 16.43*
8,9-EET	1023 ± 230.2	1078 ± 253.4	1426 ± 254.7	794.2 ± 185.0
5,6-EET	441.4 ± 52.25	542.4 ± 94.27	789.1 ± 95.48	413.3 ± 59.73*

Supplementary Table S2 gene expression quantification. mRNA expression (-Δct) in colons of control female (F-CTRL), prenatal stress female (F-PS), control male (M-CTRL) and prenatal stress male (M-PS) mice. Data are expressed as mean ± SEM. Statistical analysis was performed independently for each sex using a Mann-Whitney test. * P<0.05 compared to M-CTRL group.

	Mean ± SEM F-CTRL	**Mean ± SEM F-PS**	**Mean ± SEM M-CTRL**	**Mean ± SEM M-PS**
Alox15	-4.80 ± 0.23	-5.03 ± 0.24	-5.98 ± 0.41	-5.34 ± 0.27
Alox5	-6.79 ± 0.08	-6.80 ± 0.12	-7.07 ± 0.18	-6.87 ± 0.09*
Ptgs1	-2.65 ± 012	-2.68 ± 0.08	-2.46 ± 0.13	-2.44 ± 0.11
Ptgs2	-4.32 ± 0.11	-4.22 ± 0.25	-4.00 ± 0.21	-4.20 ± 0.20
Alox12	-8.20 ± 0.19	-7.82 ± 0.23	-7.94 ± 0.30	-8.01 ± 0.19
Penk	-4.65 ± 0.13	-4.82 ± 0.13	-4.80 ± 0.29	-4.73 ± 0.11
Ccl5	-6.31 ± 0.23	-6.56 ± 0.15	-6.41 ± 0.22	-6.44 ± 0.15
Ifng	-13.96 ± 0.34	-13.47 ± 0.35	-13.89 ± 0.36	-13.56 ± 0.21
Tgfb	-2.37 ± 0.08	-2.29 ± 0.08	-1.96 ± 0.14	-1.92 ± 0.11
Il6	-8.58 ± 0.68	-8.31 ± 0.78	-7.49 ± 0.73	-7.44 ± 0.72
Il1b	-4.75 ± 0.53	-4.70 ± 0.49	-4.13 ± 0.65	-4.33 ± 0.59
Cxcl2	-5.58 ± 0.71	-5.40 ± 0.70	-4.84 ± 0.82	-5.02 ± 0.78
Tnfa	-6.03 ± 0.17	-5.90 ± 0.16	-5.56 ± 0.18	-5.81 ± 0.15
Tff3	-0.13 ± 1.19	-0.23 ± 1.21	-0.48 ± 1.43	-0.06 ± 1.21
Occludine	-0.58 ± 0.15	-0.50 ± 0.13	-0.46 ± 0.15	-0.47 ± 0.15
Nfkb	-1.25 ± 0.11	-1.07 ± 0.13	-0.94 ± 0.09	-0.86 ± 0.11
Ppara	-5.41 ± 0.25	-5.69 ± 0.28	-5.07 ± 0.25	-5.08 ± 0.20
Tjp1	-0.24 ± 0.15	-0.27 ± 0.11	0.37 ± 0.07	0.26 ± 0.10
Acot12	-11.16 ±0.10	-11.40 ± 0.12	-10.29 ± 0.44	-10.55 ± 0.48
Angptl4	-5,40 ± 0.20	-5,49 ± 0.21	-5.52 ± 0.24	-5.70 ± 0.18
Muc2	3.13 ± 0.12	3.41 ± 0.10	3.57 ± 0.27	3.30 ± 0.16
Mmp7	-5.72 ± 1.21	-5.28 ± 1.28	-4.07 ± 1.58	-5.52 ± 1.31
Cd36	-3.22 ± 0.14	-3.05 ± 0.15	-3.11 ± 0.17	-3.21 ± 0.16
Ahr	-0.68 ± 0.84	-0.85 ± 0.71	-0.13 ± 1.13	-0.86 ± 0.68
Ephx2	-1.69 ± 0.96	-1.86 ± 0.92	-1.20 ± 1.31	-2.05 ± 0.91
Reg3g	-9.35 ± 0.30	-9.37 ± 0.22	-9.22 ± 0.28	-9.35 ± 0.32

Supplementary Table S3 QPCR Primers

Transcript	Forward	Reverse
Hprt	GTTCTTTGCTGACCTGCTGGAT	CCCCGTTGACTGATCATTACAG
Alox15	TCCGGGGATGGAGAAGCTACA	TCCGCTTCAAACAGAGTGCCT
Alox5	TCTTCCTGGCACGACTTTGCTG	GCAGCCATTCAGGAACTGGTAG
Ptgs1	CACTTCTATGCTGGTGGACTATG	CTTGATGACATCCACAGCCACAT
Ptgs2	TCAAGACAGATCATAAGCGAG	AAAGGCGCAGTTTATGTTGTC
Alox12	TGTTGCCACCATGAGATGCCT	CCACCTGTGCTCACTACCTGA
Penk	CGACATCAATTTCCTGGCGT	AGATCCTTGCAGGTCTCCCA
Ccl5	ACTCCCTGCTGCTTTGCCTAC	TTCCTTCGAGTGACAAACACGA
Ifng	CAGCAACAGCAAGGCGAAA	AGCTCATTGAATGCTTGGCG
Tgfb	GACCCCCACTGATACGCCT	GCTGAATCGAAAGCCCTGTA
Il6	TCTGGGAAATCGTGGAAATGAG	TTCTGCAAGTGCATCATCGTTG
Il1b	ACCTTCCAGGATGAGGACATGAG	CATCCCATGAGTCACAGAGGATG
Cxcl2	AGCCCCCCTGGTTCAGAAA	TCCAGGTCAGTTAGCCTTGCC
Tnfa	CCACGCTCTTCTGTCTACTGAAC	GGTCTGGGCCATAGAACTGATG
Tff3	TGCAGATTACGTTGGCCTGTC	TGGAGTCAAAGCAGCAGCC
Ocln	TGGATGACTACAGAGAGGAGAGT	TCCTCTTGATGTGCGATAATTTGC
Nfkb	ATGGCCCATACCTTCAAATAT	TCTCACTAGAGGCTCCCGGAA
Ppara	CCCTGTTTGTGGCTGCTATAATTT	GGGAAGAGGAAGGTGTCATCTG
Tjp1	GTTGGTACGGTGCCCTGAAAGA	GCTGACAGGTAGGACAGACGAT
Acot12	GGTGGTAAATGGAGACAAAC	ACGGCAGCACAACTGACCTTA
Angptl4	CTCCCAACGCCACCCACTTA	GCTGGATCTGGAAAAGTC
Muc2	CGGAACTCCAGAAAGAAGCCA	GGCAGTCAGACGCAAAGTTGTA
Mmp7	ACTGATGGTGAGGACGCAGG	CATCACAGTACCGGGAACAGAA
Cd36	ATGACGTGGCAAAGAACAGC	GAAGGCTCAAAGATGGCTCC
Ahr	CGCTTGATTTACAGAAATGGA	ATCTCGTACAACACAGCCTC
Ephx2	CGTTTATGCCACCAGATCCTGAT	ATGTTCTTCTCCAGTTCAGCCT
Reg3g	CCTCCATGATCAAAAGCAGTGG	GGATTCGTCTCCCAGTTGATGT
Nr3c1	TGGAGAGGACAACCTGACTTCC	ACGGAGGAGAACTCACATCTGG

Supplementary Table S4 Primers and probes used for TaqMan® real-time PCR assays

Target strain	Forward primer, reverse primer and probe sequence (5' - 3') *	Tm (°C)	Amplicon size (bp)
L. animalis DSMZ 20602	CTTTGCACGCAGGAGGTC	56	131
	CGCGGTGTTCTCGGTTATTT	56	
	FAM-ACGGTTCGATCCCGTTAAGCTCCA-TAMRA	62	
L. murinus IRSD_2020	CAAGAGAGTCGCTTACCAGAT	54	120
	ACCGATCTCATCTGCTGGTAG	56	
	FAM-CACCCGAAACAGTTGCAAAGCCTCT-TAMRA	62	

* FAM, 6-*carboxyfluorescein; TAMRA, tetramethylrhodamine*

Supplementary Table S5 SRM characterization with quantitative and qualitative transition, energy applied to generate the transition (EC et Q1/Q3PreBias), and retention time.

Compound	Quantitative MRM transition	Q1 Pre Bias (V)	EC (eV)	Q3 Pre Bias (V)	Qualitative transition	Retention time (min)
C12AlaGABA	384 → 366	30	11	18	384 → 102	6.3
C14AsnGABA	426 → 102	21	13	17	426 → 114	7.56
C14:1AlaGABA	381 → 102	27	31	25	381 → 88	7.82
C12ValGABA	383 → 280	12	31	27	383 → 102	8.28
C12LeuGABA	397 → 130	19	31	18	397 → 102	9.00
C14GABA	312 → 226	24	21	12	312 → 102	9.96
C14IleGABA	425 →130	22	31	20	425 → 102	11.23
C16LeuGABA	453 →130	18	34	17	453 → 130	13.53
C16PheGABA	487 → 384	19	27	19	487 → 102	13.72
C16GluGABA	465 → 102	23	37	10	465 → 96	9.13

Supplementary figures

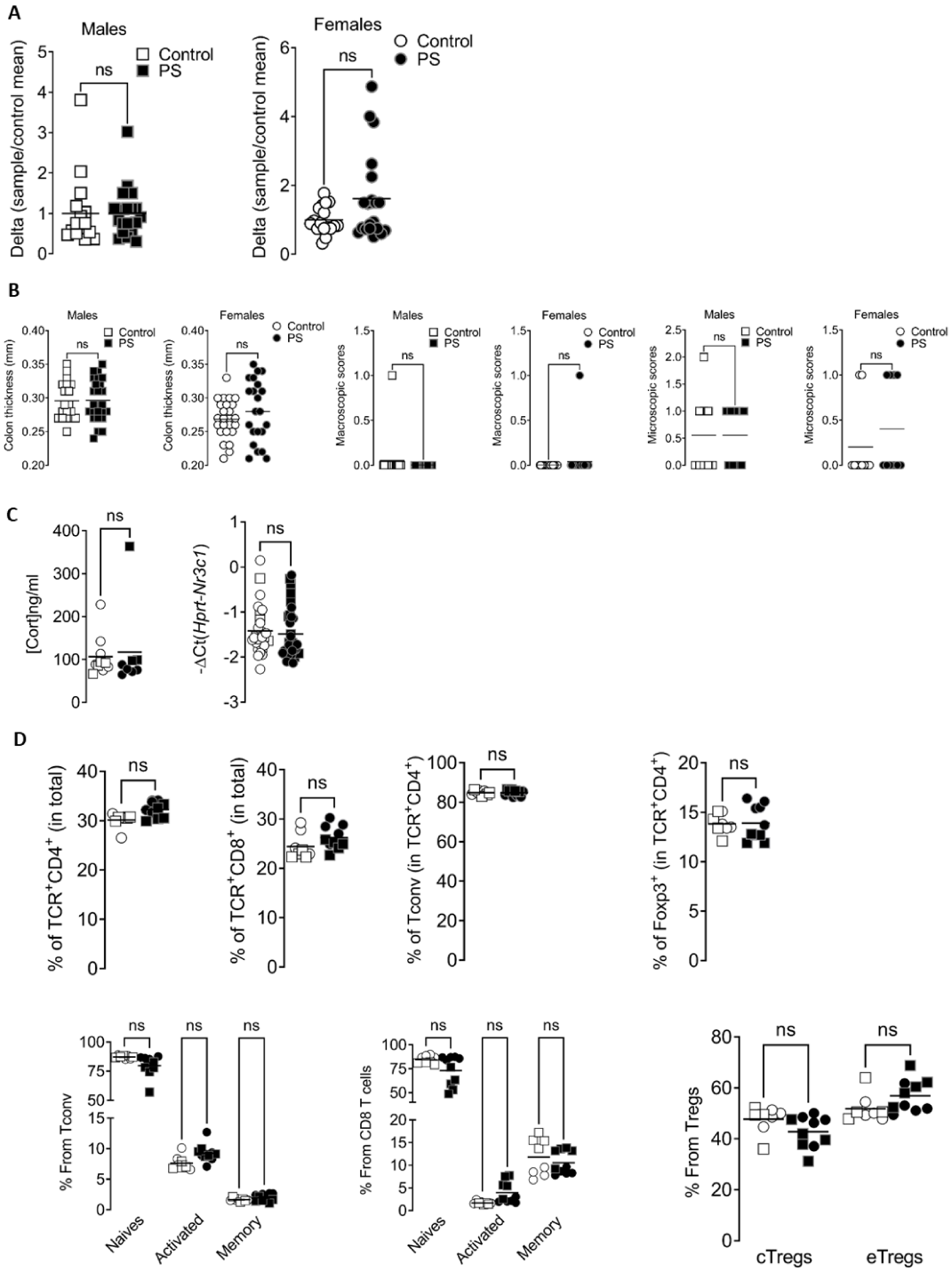

Figure S1:

(A) Intestinal paracellular permeability was monitored 4 hours after oral administration of FITC dextran 4 kDa. FITC fluorescence was quantified in the serum of control mice (white) or

PS mice (black), in the male (square) and female (circle) offspring. Data are expressed as scatter dot plot with the mean. Statistical analysis was perform using a Mann-Whitney test. (n=12-22 mice/group, 3 independent experiments). **(B)** Colon thickness, macroscopic and microscopic colon damage scores of control mice (white) or PS mice (black), in the male (square) and female (circle) offspring. Data are expressed as scatter dot plot with the mean (ctrl male vs PS male and Ctrl female vs PS female; n= 10-24 mice/group, 3 independent experiments). **(C)** Plasmatic corticosterone concentration and its receptor expression in the colon were determined in control mice (white) or prenatal stress (PS) mice (black), in the male (square) and female (circle) offspring. Data are expressed as scatter dot plot with the mean. ns: not significant. **(D)** 14 weeks old males (square) and females (circle) controls (while symbols, n=8) or prenatally stressed (black symbols, n=10) were euthanized and their mesenteric lymph node cells were analyzed by flow cytometry. The upper panel represent the proportion of the different major T cell populations in individual mice. The lower panel represent the activation status of T cell populations based on their expression of CD62L and CD44. Data are expressed as scatter dot plot with the mean. ns: not significant.

A

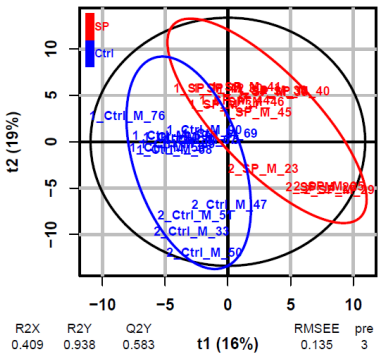

B

Variable	FDR
Colorectal distension total AUC	0.029
14,15-EET	0.033
11,12-EET	0.046
5,6-EET	0.046
L.murinus/animalis	0.046
Erysipelotrichia unknown	0.046
Desulfovibrio sp	0.046
Bacteria unclassified	0.0033

C

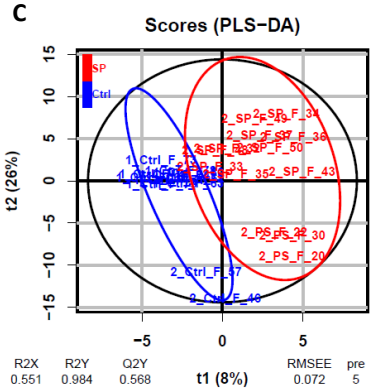

D

Variable	FDR
Colorectal distension total AUC	0.012
Clostridiales unknown	0.012
Akkermansia muciniphila	0.0042

Figure S2. PS and Ctrl mice separation in PLS-DA can be explained by visceral pain sensitivity and different bacterial abundances in male and female. Multivariate analysis of the male cohort **(A, B)** and female cohort **(C, D)**: **(A-C)** Two-dimensional PLS-DA score plots for **(A)** males ((R2X = 40.9%, R2Y = 93.8%, Q2=0.583), 28 samples (control, n = 14, blue; PS, n = 14, red)) and **(C)** females ((R2X = 55.1%, R2Y = 98,4%, Q2=0.568), 25 samples (control, n = 12, blue; PS, n = 13, red)). Each dot corresponds to an individual. The black ellipse corresponds to a 95% confident interval based on the Hotelling's T^2. **(B-D)** Discriminant (Variable Importance in Projection > 1) and significant (FDR-corrected p value of Wilcoxon test < 0.05) variables for male **(B)** and female **(D)**.

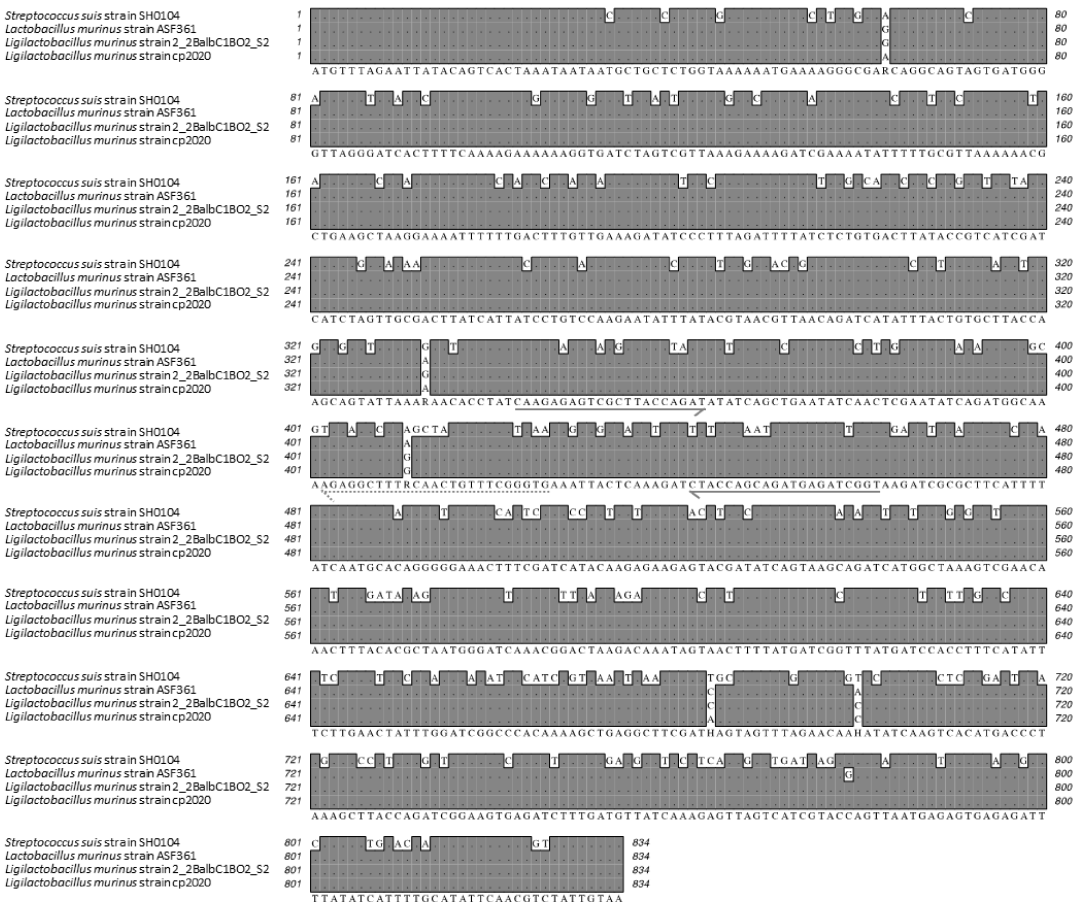

Figure S3. Primers and probe designed for the *L. murinus* specific real-time PCR assay. The nucleotide sequence of an open reading frame (ORF) identified in the *L. murinus* strain IRSD_2020 was aligned with those of a nearly identical ORF found in *L. murinus* strains ASF361 and 2_2BalbC1BO2_S2, and an ORF with less than 77% similarity found in *Streptococcus suis* strain SH0104. Identical and different nucleotides are reported with grey and white background, respectively. Solid and dashed arrows (5' to 3' orientation) indicate the positions of the primers and probe, respectively, which were selected in locations displaying nucleotide variability, in order to specifically target *L. murinus* IRSD_2020 by real-time PCR.

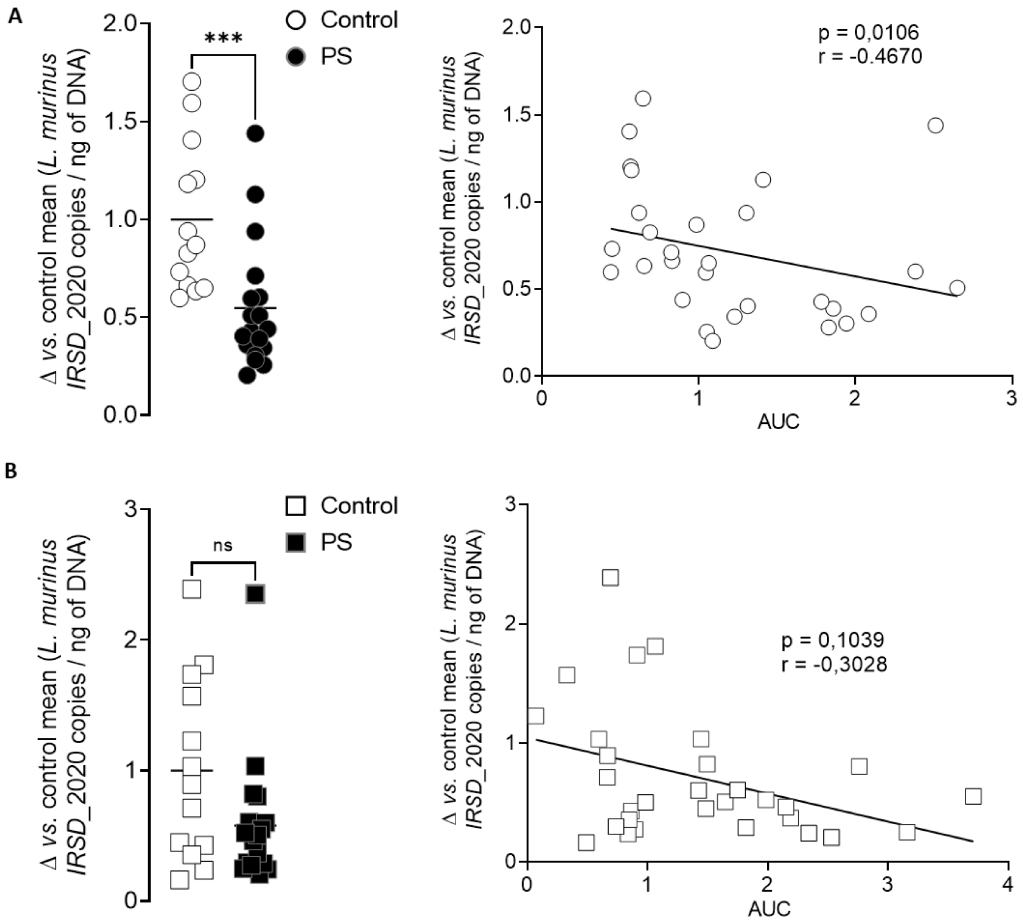

Figure S4: *L. murinus* IRSD_2020 concentration is decreased in PS female mouse feces

The levels of the *L. murinus* strain IRSD_2020 were quantified by TaqMan® real-time PCR in the feces of control mice (white) or PS mice (black), in the female (**A**, circle) and male (**B**, square) offspring. Data are expressed as scatter dot plot with the mean. Statistical analysis was performed using a Mann-Whitney test. ***p<0.001, significantly different from the control group (n=13-18 male mice/group and n=14-18 female mice/group, 3 independent experiments). Spearman correlations were used to analyze the correlation between the fecal bacteria quantity and visceral motor response to colorectal distension expressed in AUC, in male (square) and female (circle) offspring. P and r values are indicated on each graph.

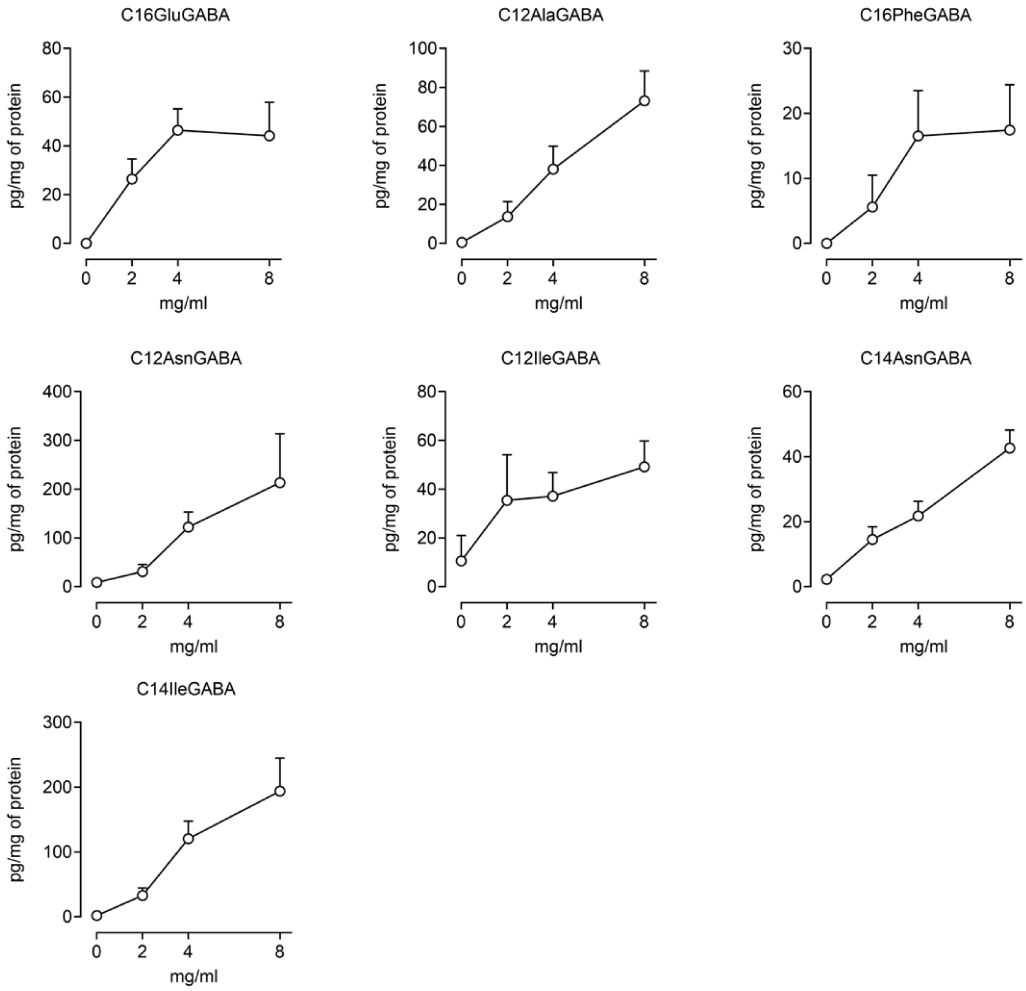

Figure S5*. L. murinus* IRSD_2020 produces GABA-lipopeptides. Concentration of lipopeptides quantified by LC-MS/MS in the bacterial pellets of *L. murinus* IRSD_2020 cultivated without (0 mg/mL) or with GABA (2, 4 or 8 mg/mL). Data are expressed as scatter dot plot with the mean (n=9).

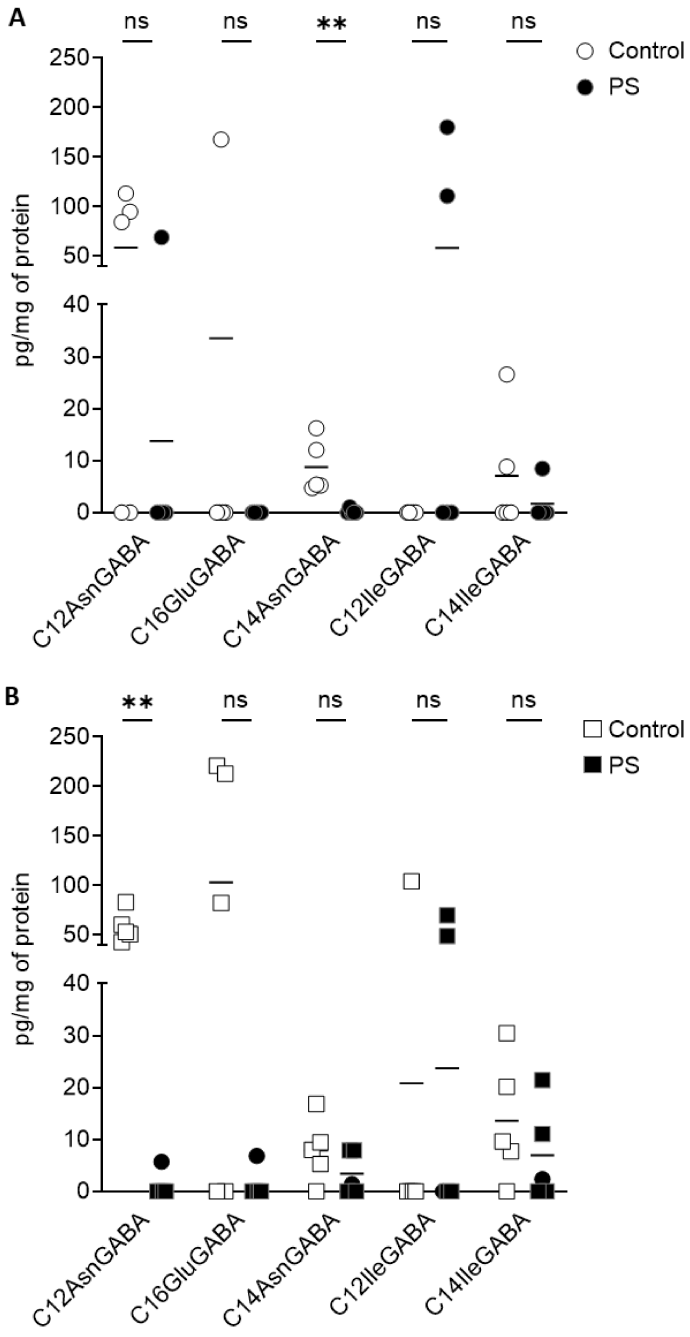

Figure S6: Concentration of C12AsnGABA and of C14AsnGABA is decreased in PS female and PS male mouse, respectively. (B) Individual (left panel) and total (right panel) concentration of lipopeptides quantified by LC-MS/MS in the colon of female (**A**, circle) and male (**B**, square) control (white) and PS mice (black). Data are expressed as scatter dot plot with the mean (n=5 female mice and n=4-5 male mice). Statistical analysis was performed using a Mann-Whitney test. *p<0.05, **p<0.01, significantly different from the corresponding control group

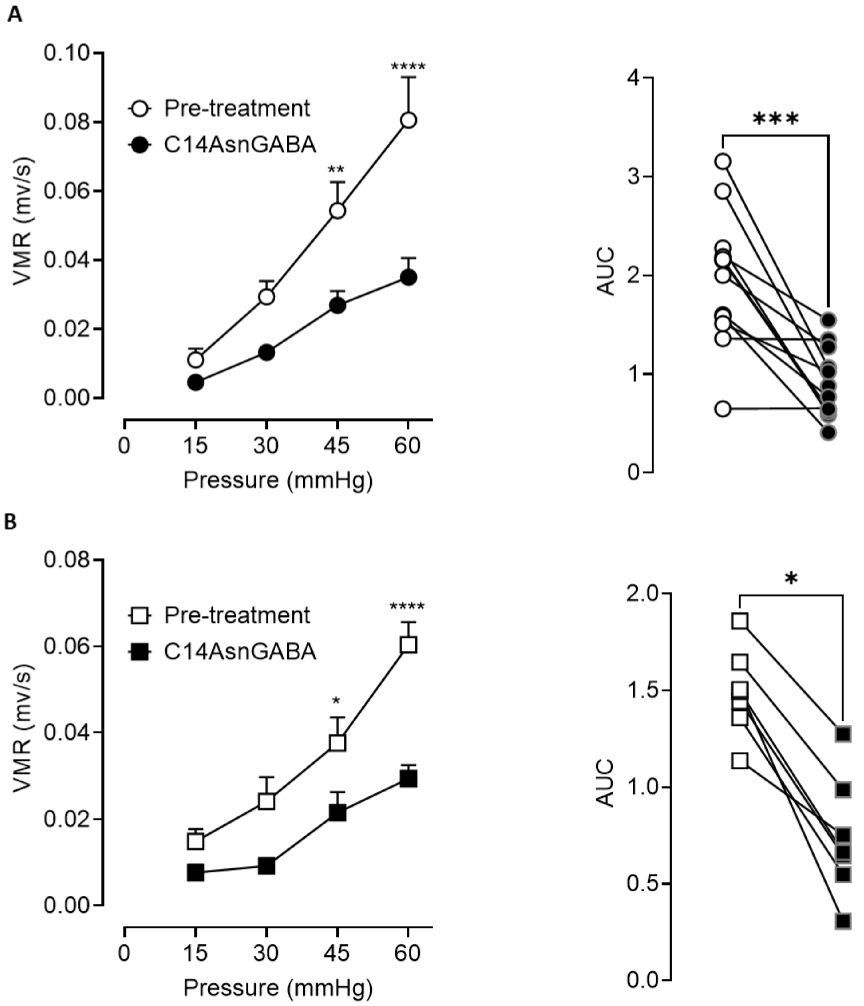

Figure S7: C14AsnGABA administration decrease PS-induced visceral hypersensitivity in male and female mice. Visceral motor response to colorectal distensions (VMR) in response to increasing pressures of distension (15, 30, 45 and 60 mmHg) was measured, in both female (**A**) and male (**B**) PS offspring. Measurements were done before (white) and after intracolonic administrations of C14AsnGABA (black). Data are expressed as mean ± SEM (n=12 female mice/group and n=7 male mice/group, 2 independent experiments mixing male and female). Statistical analysis was performed using two-way Anova analysis of variance and subsequent Sidak's multiple comparison test. *P<0.05, **p<0.01, ****p<0.0001 significantly different from pretreatment group. The results are also expressed as area under the curve (AUC) presented as scatter dot plot with the mean. Statistical analysis was perform using a Wilcoxon test. *P<0.05, ***p<0.001, significantly different from the pretreatment group.

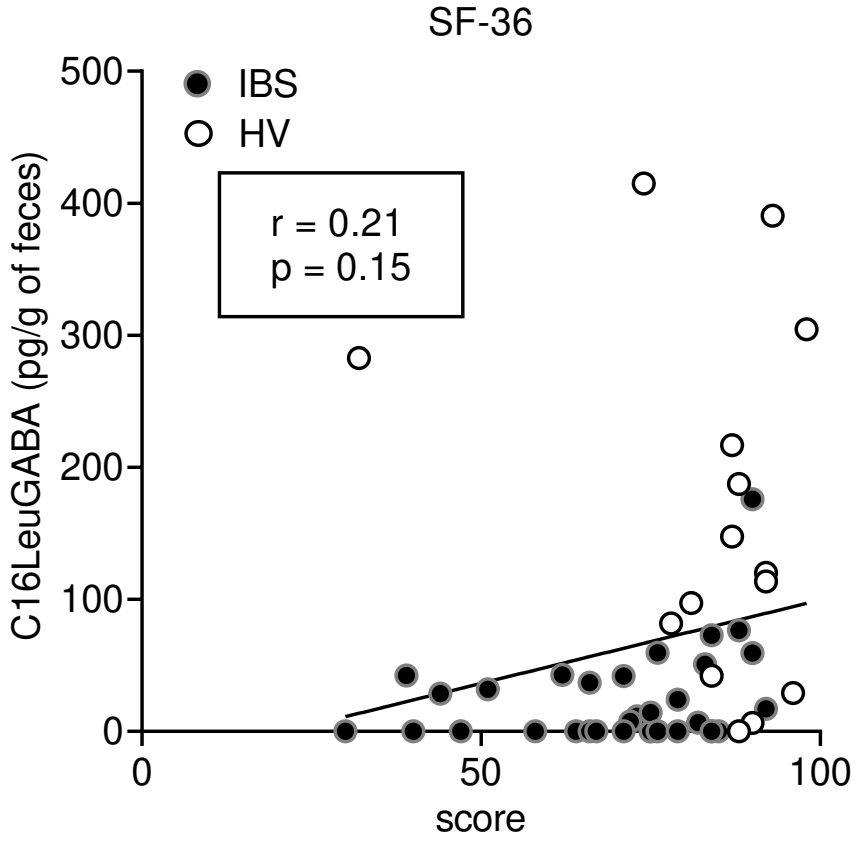

Figure S8. Correlation between C16LeuGABA in feces and SF-36 score. Spearman correlation was used to analyse the correlation between the concentration of CL16LeuGABA and SF-36 score in healthy volunteers (HV, white) and patients with IBS (black). p and r values are indicated on the graph

Supplementary references

[1] J. Boué *et al.*, « Endogenous regulation of visceral pain via production of opioids by colitogenic CD4(+) T cells in mice », *Gastroenterology*, vol. 146, nº 1, p. 166-175, janv. 2014, doi: 10.1053/j.gastro.2013.09.020.

[2] P. Le Faouder *et al.*, « LC-MS/MS method for rapid and concomitant quantification of pro-inflammatory and pro-resolving polyunsaturated fatty acid metabolites », *J. Chromatogr. B Analyt. Technol. Biomed. Life. Sci.*, vol. 932, p. 123-133, août 2013, doi: 10.1016/j.jchromb.2013.06.014.

[3] S. Nicolas *et al.*, « Transfer of dysbiotic gut microbiota has beneficial effects on host liver metabolism », *Mol. Syst. Biol.*, vol. 13, nº 3, p. 921, mars 2017, doi: 10.15252/msb.20167356.

[4] N. Segata *et al.*, « Metagenomic biomarker discovery and explanation », *Genome Biol.*, vol. 12, nº 6, p. R60, juin 2011, doi: 10.1186/gb-2011-12-6-r60.

[5] M. G. I. Langille *et al.*, « Predictive functional profiling of microbial communities using 16S rRNA marker gene sequences », *Nat. Biotechnol.*, vol. 31, nº 9, p. 814-821, sept. 2013, doi: 10.1038/nbt.2676.

[6] O. Hammer, D. A. T. Harper, et P. D. Ryan, « PAST: Paleontological Statistics Software Package for Education and Data Analysis », p. 9.

[7] T. Pérez-Berezo *et al.*, « Identification of an analgesic lipopeptide produced by the probiotic Escherichia coli strain Nissle », *Nat. Commun.*, vol. 8, nº 1, déc. 2017, doi: 10.1038/s41467-017-01403-9.

[8] A. Hueber *et al.*, « Identification of bacterial lipo-amino acids: origin of regenerated fatty acid carboxylate from dissociation of lipo-glutamate anion », *Amino Acids*, vol. 54, nº 2, p. 241-250, févr. 2022, doi: 10.1007/s00726-021-03109-1.

[9] A. Hueber *et al.*, « Discovery and quantification of lipoamino acids in bacteria », *Anal. Chim. Acta*, vol. 1193, p. 339316, févr. 2022, doi: 10.1016/j.aca.2021.339316.

[10] N. Cenac *et al.*, « Potentiation of TRPV4 signalling by histamine and serotonin: an important mechanism for visceral hypersensitivity », *Gut*, vol. 59, nº 4, p. 481-488, 2010, doi: 10.1136/gut.2009.192567.

[11] E. A. Thévenot, A. Roux, Y. Xu, E. Ezan, et C. Junot, « Analysis of the Human Adult Urinary Metabolome Variations with Age, Body Mass Index, and Gender by Implementing a Comprehensive Workflow for Univariate and OPLS Statistical Analyses », *J. Proteome Res.*, vol. 14, nº 8, p. 3322-3335, août 2015, doi: 10.1021/acs.jproteome.5b00354.

[12] Y. Guitton *et al.*, « Create, run, share, publish, and reference your LC-MS, FIA-MS, GC-MS, and NMR data analysis workflows with the Workflow4Metabolomics 3.0 Galaxy online infrastructure for metabolomics », *Int. J. Biochem. Cell Biol.*, vol. 93, p. 89-101, déc. 2017, doi: 10.1016/j.biocel.2017.07.002.